CHAPTER III
RESULTS AND DISCUSSION

3.1 Flow Curves

Figures 3.1-3.10 show flow curves, plots of the wall shear stress (τ_w) versus the apparent strain rate (γ_a), for HDPE/PP (P340J) blends of ratios 100/0, 80/20, 70/30, 60/40, 50/50, 40/60, 30/70, 20/80, 0/100 and HDPE/PP (P400S) blend of ratio 70/30 respectively. In each flow curve, we divided the flow curve into several regimes; each regime is identified by either an extrudate skin texture or an oscillation of the load required to extrudate the melt through the capillary.

For pure HDPE shown in Figure 3.1, there are 5 regimes identifiable. Regime I corresponds to an extrudate with a glossy smooth skin, it ends at the apparent strain rate of 86.6 (1/s). Regime II is identified with a sharkskin texture, it terminates at the apparent strain rate of 297.8 (1/s). Regime III is called an oscillating regime because the load required to push the barrel piston at a constant speed fluctuated. The extrudate had a mixed skin texture consisting to a sharkskin segment, a glossy smooth skin segment and a melt fracture segment. For each cycle of load fluctuation, we observed that the sharkskin and the glossy segments were extruded when the load was rising, and the melt fracture segment appeared when the load was descending. At a higher strain rate but still in the regime III, we observed that the sharkskin segment became shorter, the melt fracture segment was longer but the glossy smooth segment remained the same. Regime III terminates at the apparent strain rate of 1478 (1/s). Regime IV was observed with an appearance of a peeled orange in

which we have assigned this name because of the skin waviness. It is considered to be a long wavelength instability because the skin wavelength is comparable to or longer than the extrudate diameter. This regime ends at the apparent strain rate of 2761 (1/s). Regime V covers the portion of the flow curve when a melt fracture extrudate occurs.

For pure PP (P340J) , we identified only two regimes as shown in Figure 3.2: a glossy smooth skin and a peeled orange texture. We found that load fluctuation did not occur for pure PP. For the HDPE/PP(P340J) blends of various composition ratios, we have identified regimes according to the skin textures as shown in Figures 3.3 - 3.10. The regimes identified with skin textures for all materials studied are summarized in Table 3.2.1 We note that regime V, if it appears, is always accompanied with a melt fracture surface and is proceeded by regime IV whose skin texture must be quite different. Regime IV is always a regime which follows an oscillating regime; regime IV skin textures could be either a peeled orange, a ripple, a melt fracture of a mixture of a melt fracture and smooth skin.

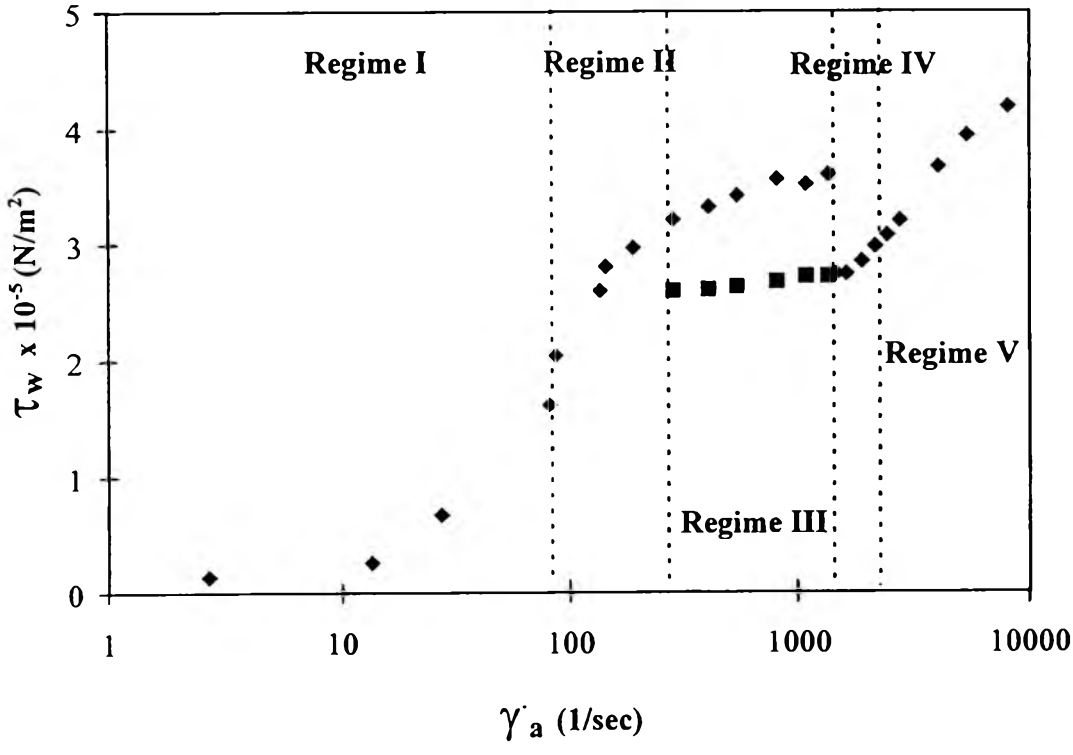

Figure 3.1 The wall shear stress, τ_w, versus the apparent strain rate, $\dot{\gamma}_a$, for HDPE/PP(P340J) blends of ratio 100/0.

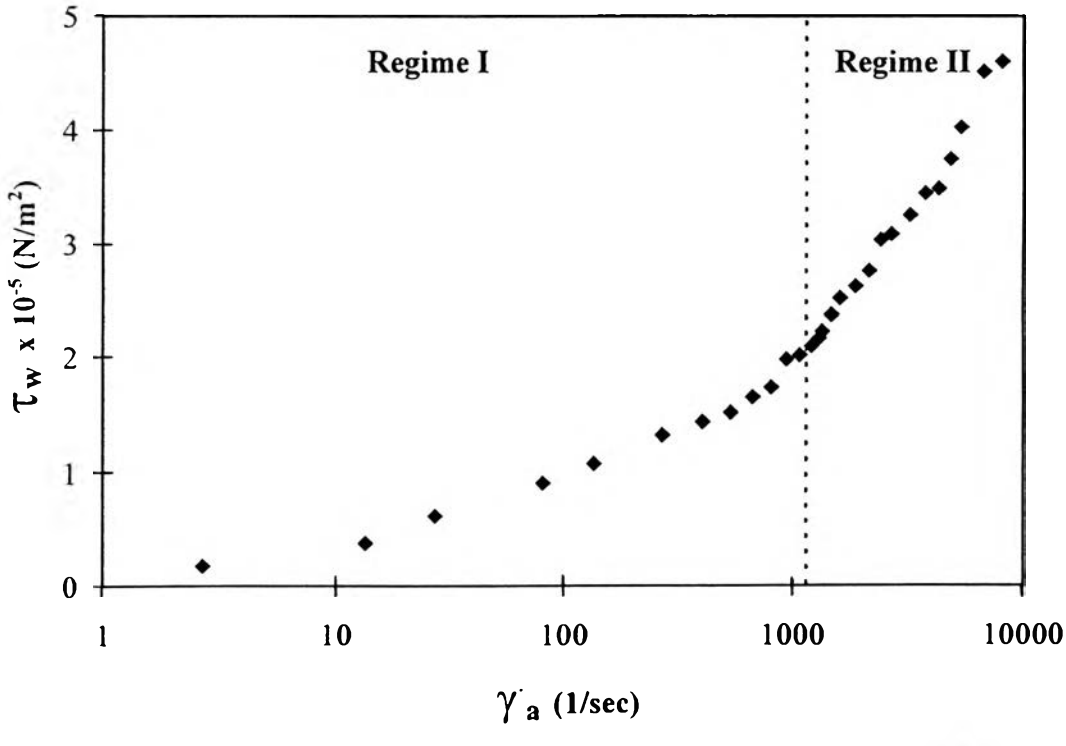

Figure 3.2 The wall shear stress, τ_w, versus the apparent strain rate, $\dot{\gamma}_a$, for HDPE/PP(P340J) blends of ratio 0/100.

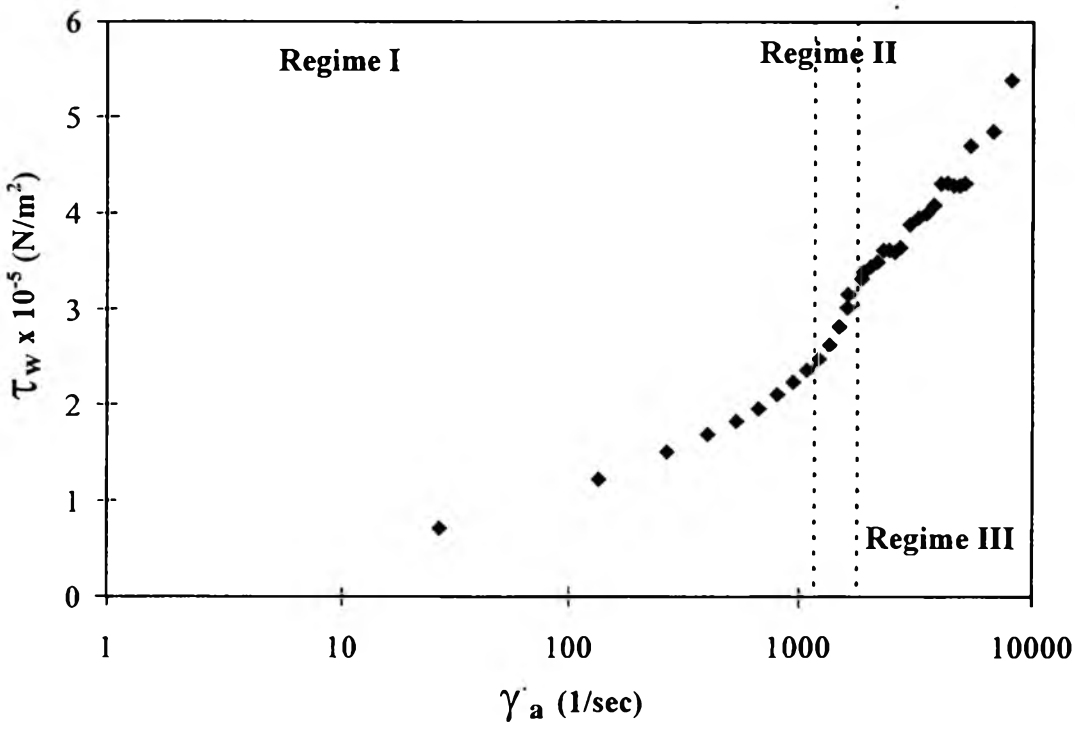

Figure 3.3 The wall shear stress, τ_w, versus the apparent strain rate, γ_a, for HDPE/PP(P340J) blends of ratio 20/80.

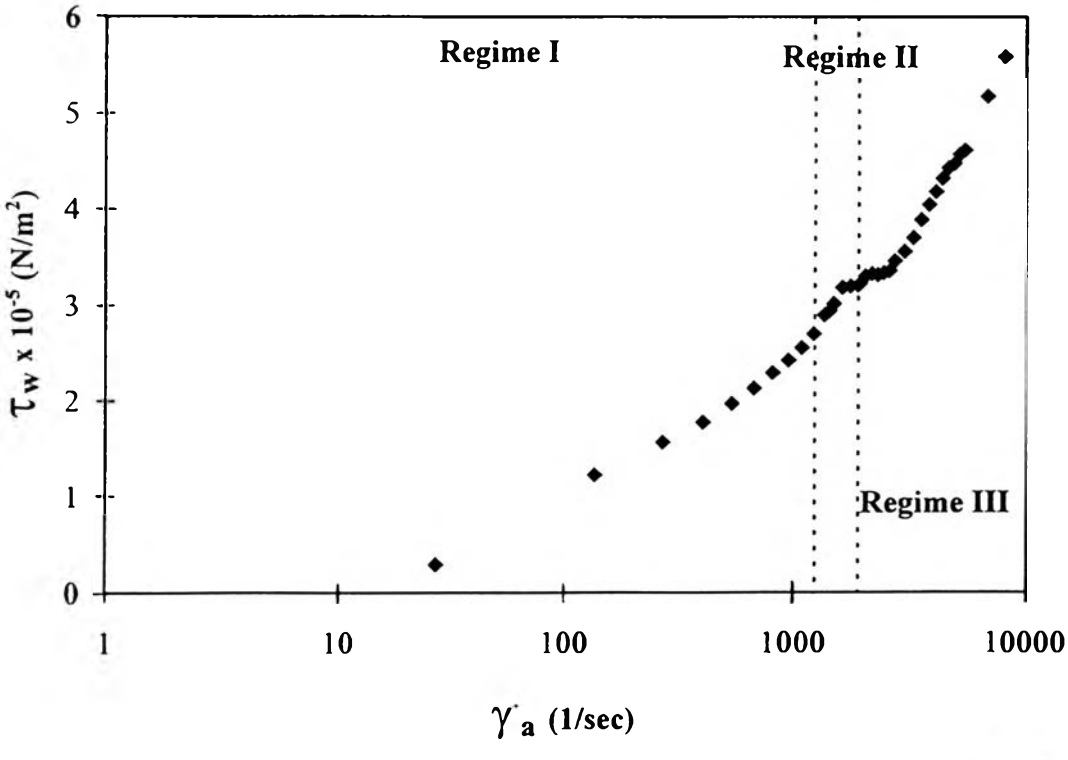

Figure 3.4 The wall shear stress, τ_w, versus the apparent strain rate, γ_a, for HDPE/PP(P340J) blends of ratio 30/70.

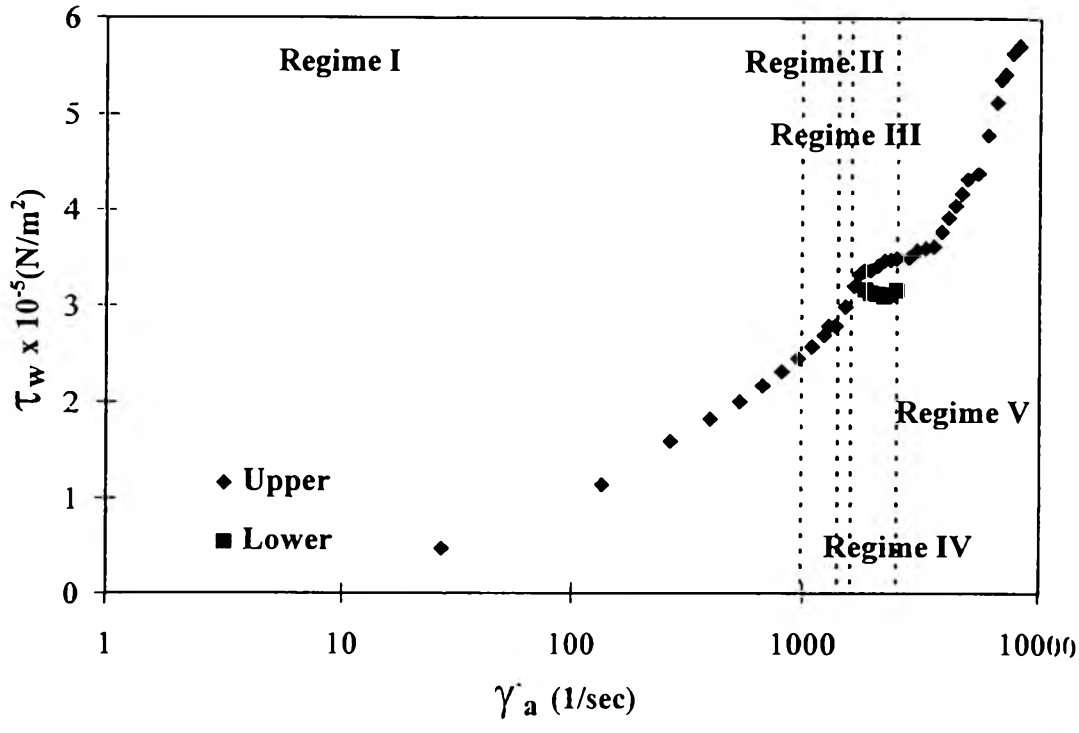

Figure 3.5 The wall shear stress, τ_W, versus the apparent strain rate, $\dot{\gamma}_a$, for HDPE/PP(P340J) blends of ratio 40/60.

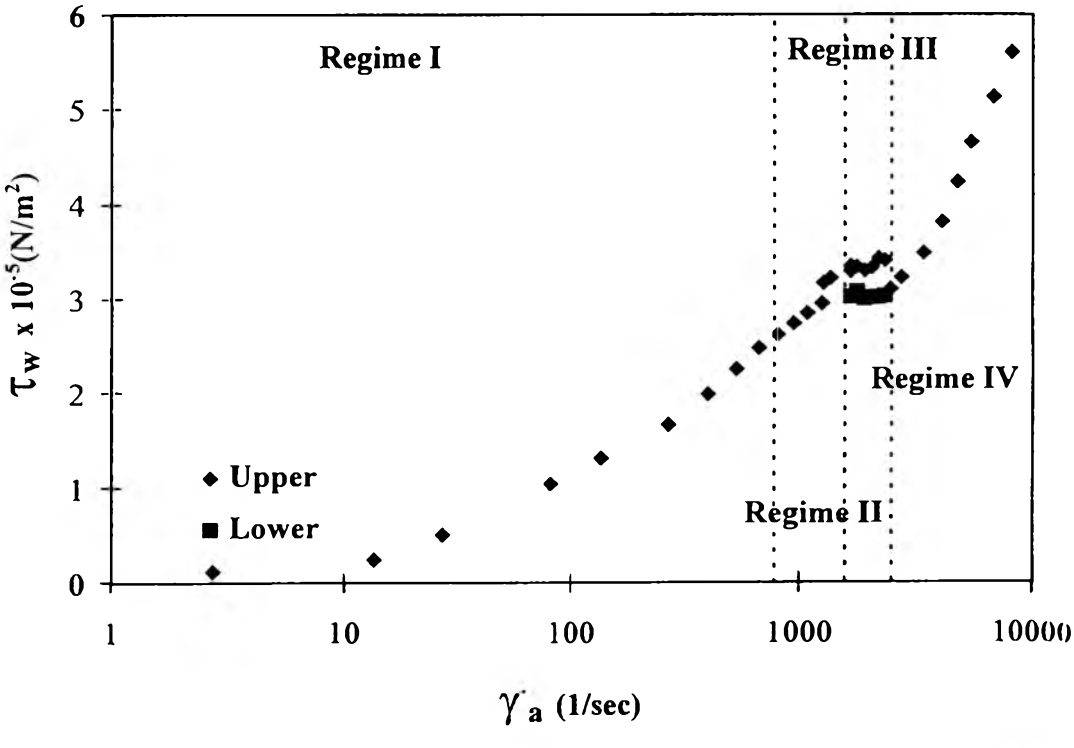

Figure 3.6 The wall shear stress, τ_W, versus the apparent strain rate, $\dot{\gamma}_a$, for HDPE/PP(P340J) blends of ratio 50/50.

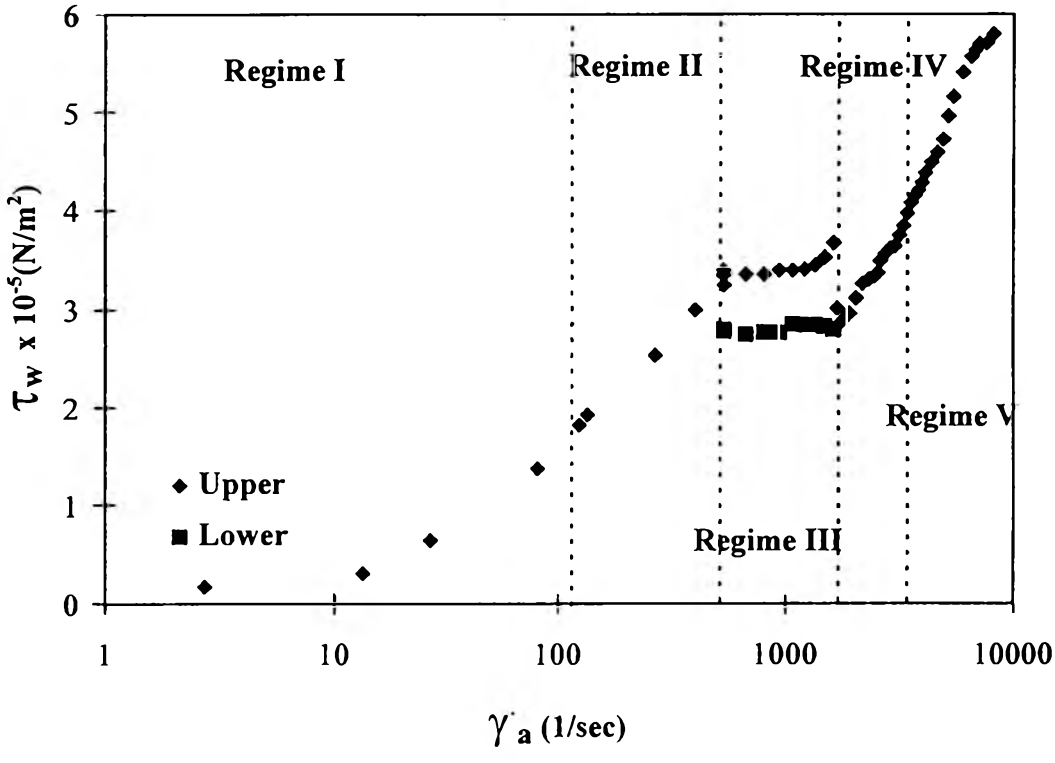

Figure 3.7 The wall shear stress, τ_w, versus the apparent strain rate, $\dot{\gamma}_a$, for HDPE/PP(P340J) blends of ratio 60/40.

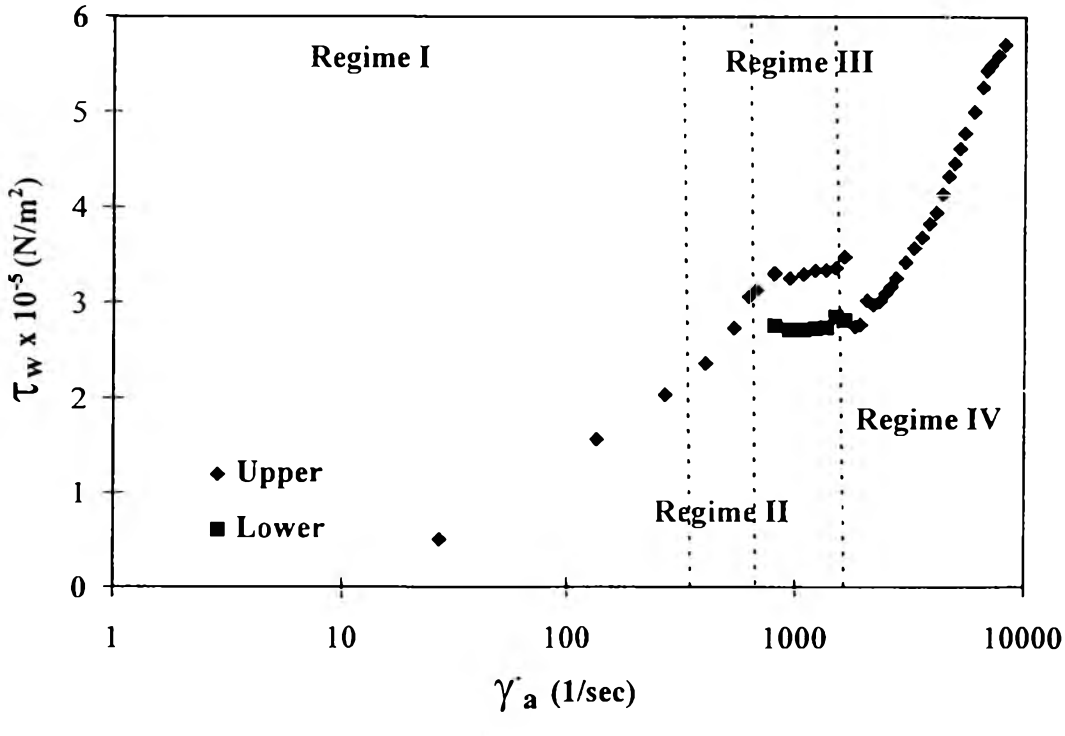

Figure 3.8 The wall shear stress, τ_w, versus the apparent strain rate, $\dot{\gamma}_a$, for HDPE/PP(P340J) blends of ratio 70/30.

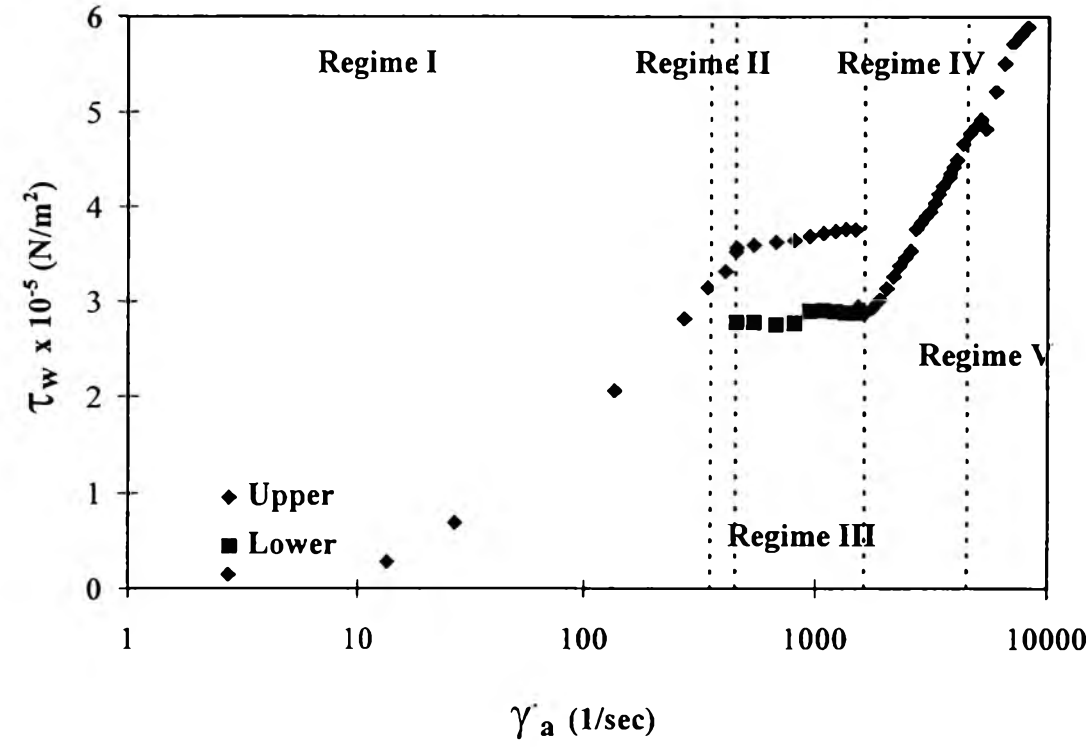

Figure 3.9 The wall shear stress, τ_w, versus the apparent strain rate, $\dot{\gamma}_a$, for HDPE/PP(P340J) blends of ratio 80/20.

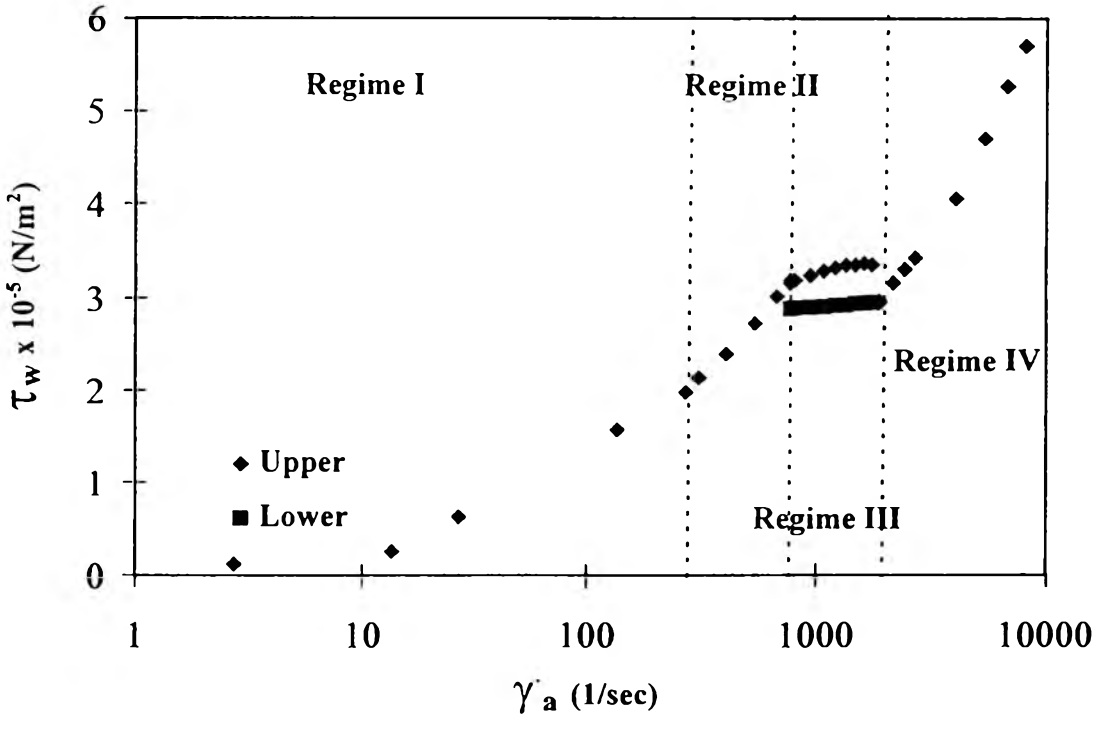

Figure 3.10 The wall shear stress, τ_w, versus the apparent strain rate, $\dot{\gamma}_a$, for HDPE/PP(P400S) blends of ratio 70/30.

3.2 Surface Textures

Now we shall attempt to describe each skin texture.

HDPE/PP(P340J): 100/0

Figures 3.11-3.15 show photographic pictures of the capillary melt extrudates from the 5 regimes identified. The melt extrudate of regime I in figure 3.11 has a surface which appears to be *glossy smooth*. The word glossy is used here to imply a shiny condition of the skin. We note that the melt flow was laminar and the melt viscosity was independent of strain rate and therefore no instability took place. A *sharkskin* texture appears in regime II as shown in Figures 3.12 (a) and (b). Here we identified a semiregular appearance of perpendicular grooves whose wavelength and amplitude are small compared to the extrudate diameter or the capillary diameter. This identification is identical to that to other previous work (Kurtz,1992). As the apparent strain rate was larger, grooves became more disordered and the surface roughness increases. Figure 3.13 (a) shows a mixture of a *sharkskin* segment and *glossy smooth* segment occurring in regime III. The descriptions of the glossy smooth and the sharkskin segments are similar to those given in the regimes I and II respectively. Figure 3.13 (b) shows a *melt fracture* segment. It consists of a surface with irregular or random roughness whose amplitude is comparable to the capillary diameter (generally above 20%). As noted previously, the melt fracture segment became longer and the sharkskin segment became shorter as the strain rate increased. In Regime IV, we found a peeled orange extrudate as shown in figure 3.14. A peeled orange skin is a surface waviness whose wavelength and amplitude are comparable to or larger than the capillary diameter. We can identify this type of skin texture to be associated with some kind of a long wavelength instability. Figure 3.15 shows the *melt fracture*

extrudate of regime V. A melt fracture is sometimes not easy to identify. It's skin has an irregular or random roughness whose amplitude is comparable to the extrudate diameter. The physical appearances of the melt fracture in this regime are deemed identical to those of regime III. Our terminology of melt fracture corresponds to the same extrudate which is sometimes called wavy roughness by several past investigators (Denn, 1990).

Figure 3.11 Stereomicroscope photograph of the glossy smooth extrudate at HDPE/PP(P340J) : 100/0. ($\dot{\gamma}_a$ = 27.07 1/sec)

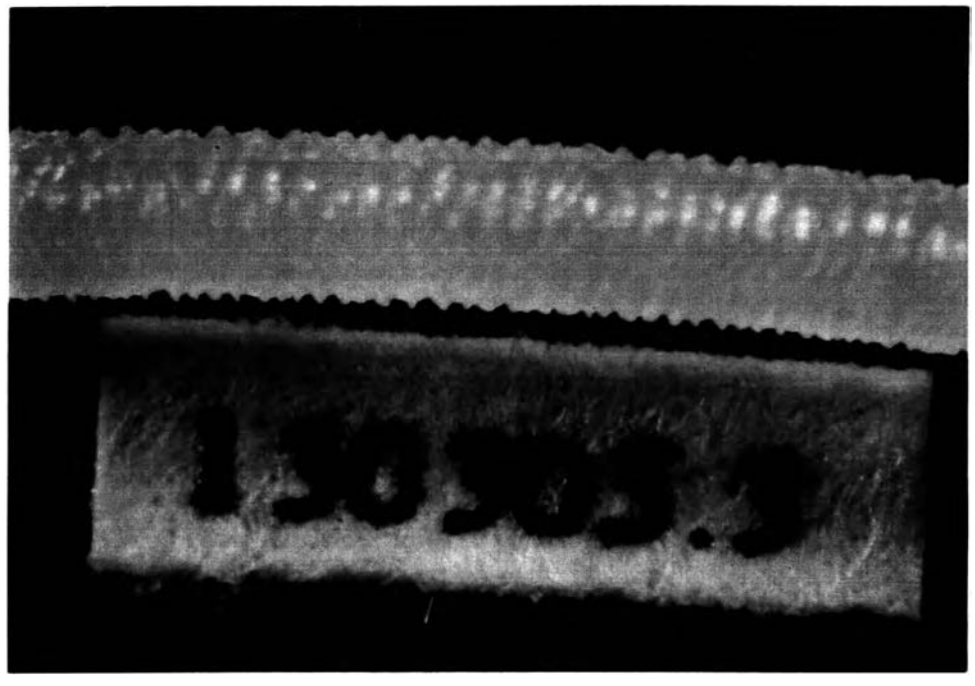

Figure 3.12a Stereomicroscope photograph of the sharkskin surface at HDPE/PP(P340J) : 100/0. ($\gamma \cdot_a$ = 143.5 1/sec)

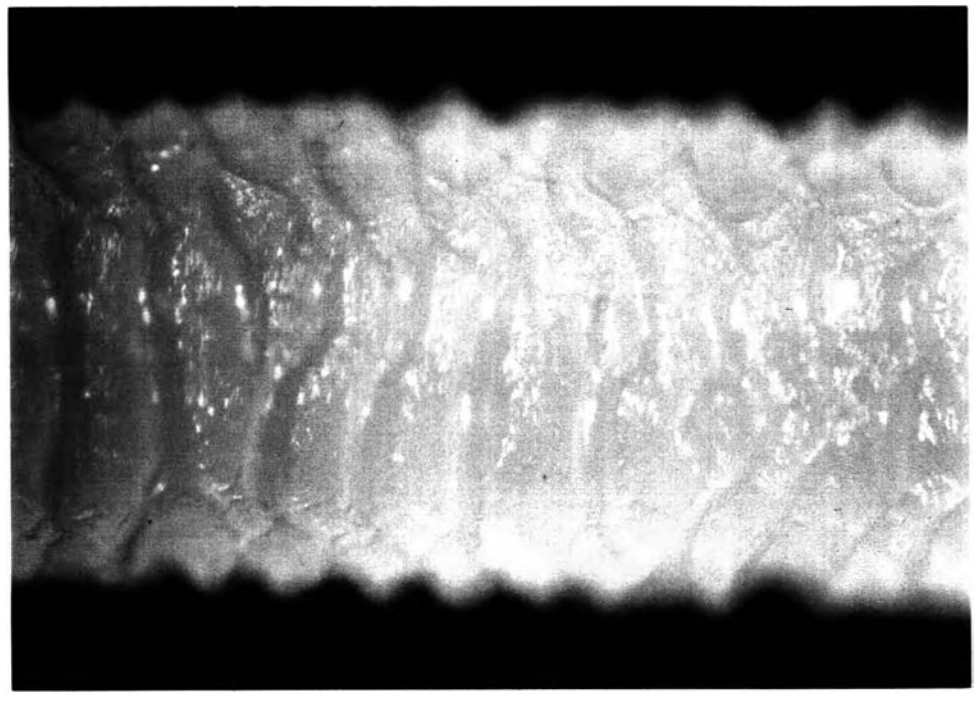

Figure 3.12b Optical microscope photograph of the sharkskin surface at HDPE/PP(P340J) : 100/0. ($\gamma \cdot_a$ = 143.5 1/sec)

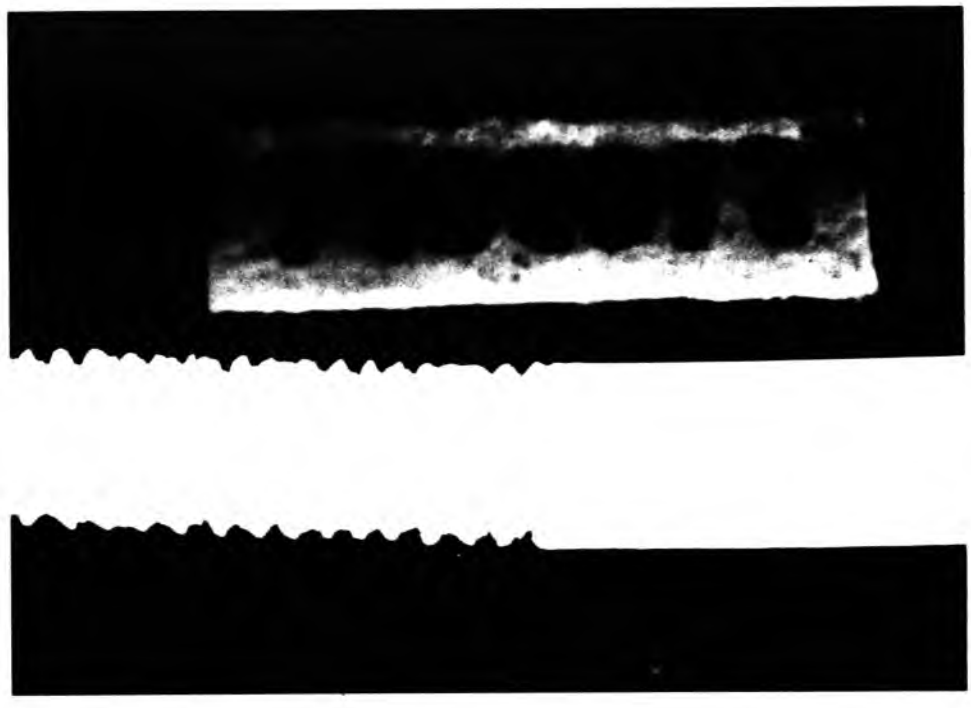

(a) Sharkskin/ Glossy smooth

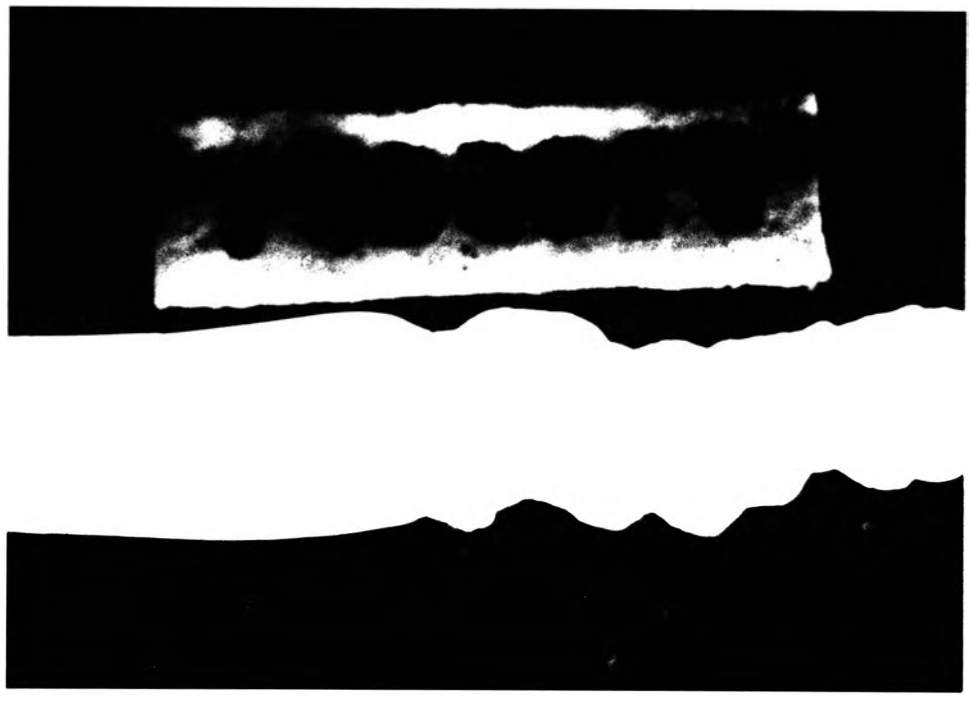

(b) Glossy smooth/ Melt Fracture

Figure 3.13 Stereomicroscope photograph of the three forms of the extrudate in the oscillation regime at HDPE/PP(P340J) : 100/0. (γ_a = 406.1 1/sec)

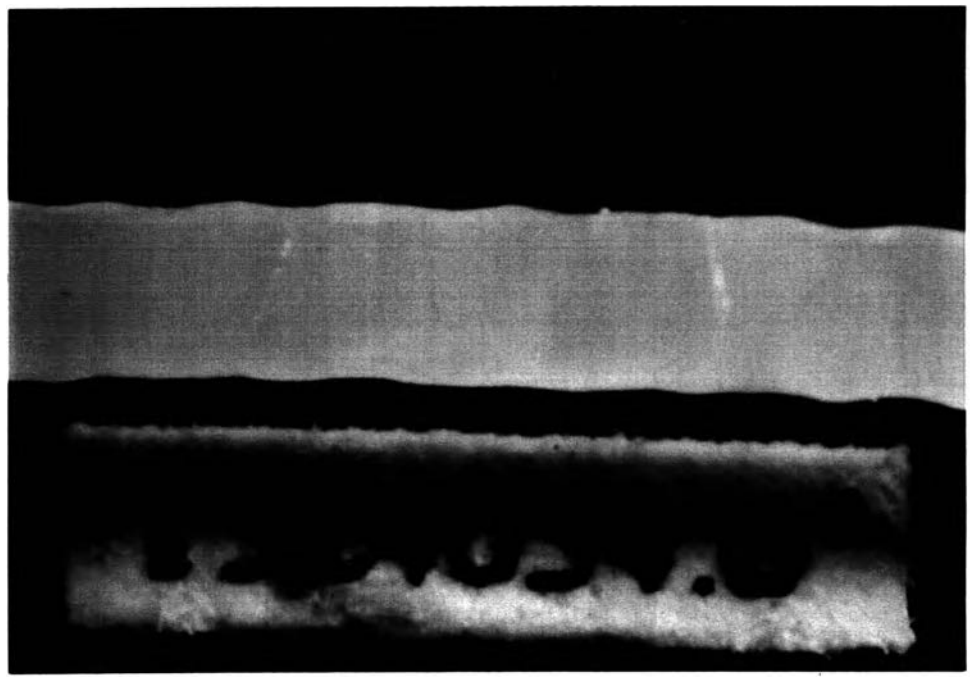

Figure 3.14 Stereomicroscope photograph of the peeled orange extrudate at HDPE/PP(P340J) : 100/0. ($\gamma \cdot_a$ = 147.8 1/sec)

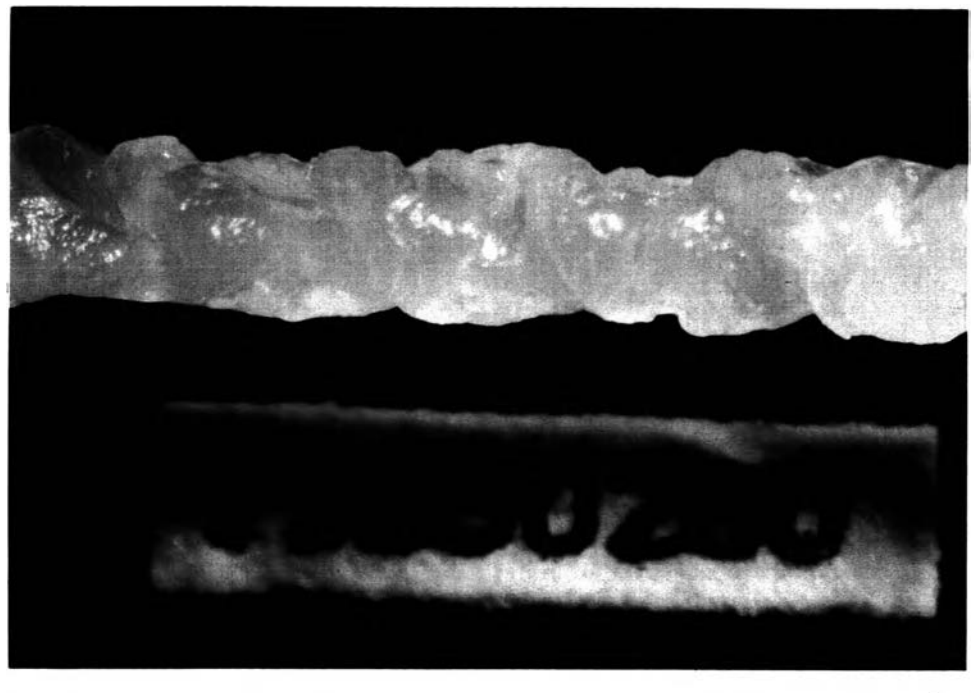

Figure 3.15 Stereomicroscope photograph of the melt fracture extrudate at HDPE/PP(P340J) : 100/0. ($\gamma \cdot_a$ = 541.4 1/sec)

HDPE/PP(P340J) : 0/100

For pure PP, we observed two regimes. Regime I skin texture was *glossy smooth* as shown in Figure 3.16. The skin descriptions are identical to those of pure HDPE with the exception of a difference in color appearance. The skin texture changes to a *peeled orange,* as shown in Figures 3.17 (a) and 3.17 (b), when we enters into regime II. The skin descriptions are the same as those of the peeled orange found for HDPE. We note here that the change in skin appearance of PP is unusual in the sense that its skin texture changes from a smooth skin (stable flow) to a surface roughness having a long wavelength (long wavelength instability). The more common situation is the case of changing from a smooth skin to a surface roughness of a short wavelength, such as the sharkskin for the pure HDPE.

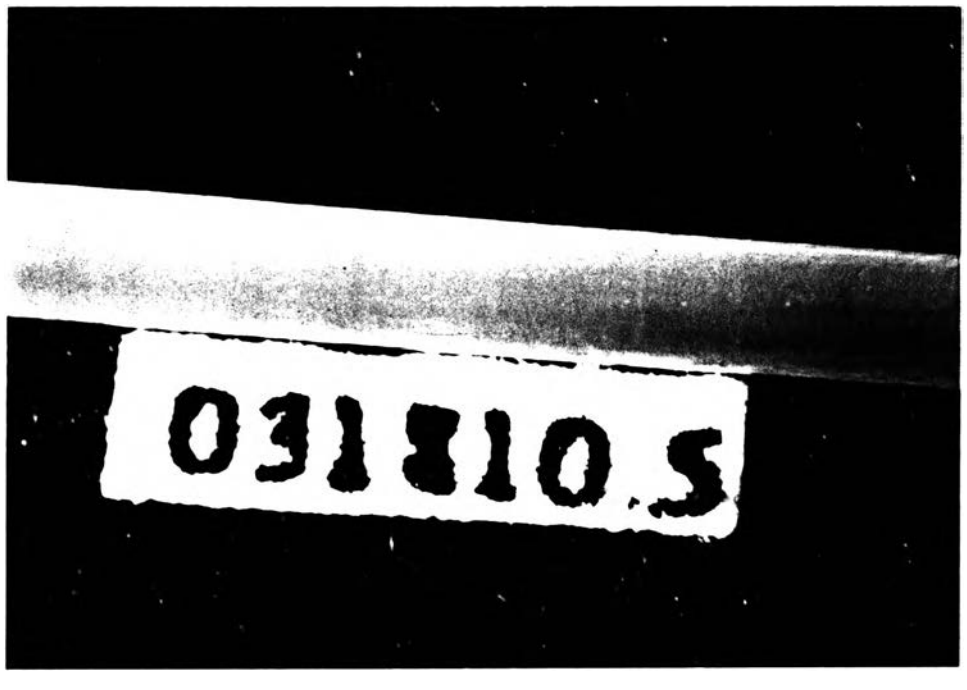

Figure 3.16 Stereomicroscope photograph of a glossy smooth extrudate at HDPE/PP(P340J) : 0/100. (γ_a = 13.54 1/sec)

Figure 3.17 (a) Stereomicroscope photograph of a small peeled orange extrudate at HDPE/PP(P340J) : 0/100. ($\gamma \cdot_a$ = 8121 1/sec)

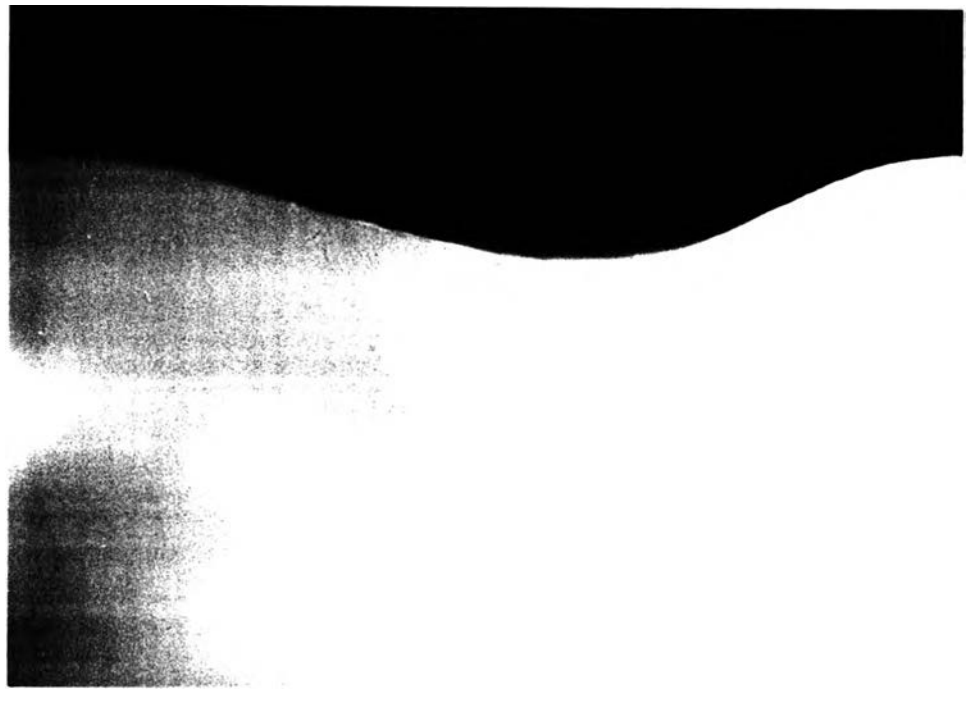

Figure 3.17 (b) Optical microscope photograph of a peeled orange extrudate at HDPE/PP(P340J) : 0/100. ($\gamma \cdot_a$ = 8121 1/sec)

The other blends

For the other blends, different surfaces or skin textures were observed and shown in Figures 3.18-3.23. Table 3.2.1 summarizes surface texture classifications as observed through the stereo and optical microscopes. Figure 3.18 shows a HDPE/PP(P3470J): 40/60 extrudate with a *hazy smooth* skin. This skin is identified as a smooth skin without a shiny appearance, which is to be differentiated from the glossy smooth skin. Figure 3.19 shows a HDPE/PP(P3470J): 80/20 extrudate with a *matteness* skin. Matteness skin refers to a surface texture with a very small roughness; it is difficult sometimes to distinguish from a sharkskin. Matteness roughness is of more order and of a smaller amplitude than that of a sharkskin. Figure 3.20 shows a HDPE/PP(P340J) : 70/30 extrudate with a *ripple* skin. This texture is different from the sharkskin in the sense that the roughness is more gentle and looks like a stack of donut. However, the wavelength is much smaller that the extrudate diameter. Figure 3.21 shows a HDPE/PP(P340J) : 60/40 with a *small scale roughness* skin. This skin is different from the melt fracture because its roughness is of less severity, and from the peeled orange because its roughness has no order. Figure 3.22 shows a HDPE/PP(P340J) : 30/70 extrudate with a *helix* surface. The roughness amplitude is comparable to the extrudate diameter whereas the wavelength is larger than the extrudate diameter. The main difference from the peeled orange is the direction of the disturbance wave vector; for the peeled orange, the wave vector is along the flow direction whereas for the helix the wave vector is at an oblique angle to the flow direction. Finally we show pictures of a ripple/hazy smooth extrudate and a melt fracture/glossy smooth in Figures 3.23 (a) and 3.23 (b) respectively. The descriptions of these skin textures are the same as those given previously.

Figure 3.18 Stereomicroscope photograph of a hazy smooth extrudate at HDPE/PP(P340J) : 70/30. ($\gamma \cdot_a$ = 270.7 1/sec)

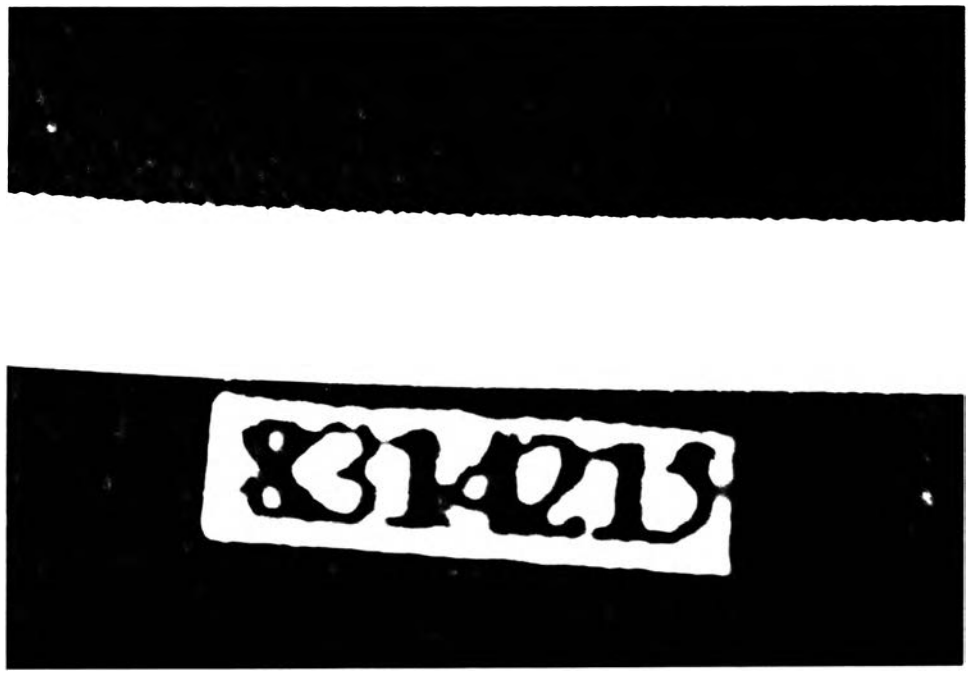

Figure 3.19 Stereomicroscope photograph of a matteness extrudate at HDPE/PP(P340J) : 80/20. ($\gamma \cdot_a$ = 406.1 1/sec)

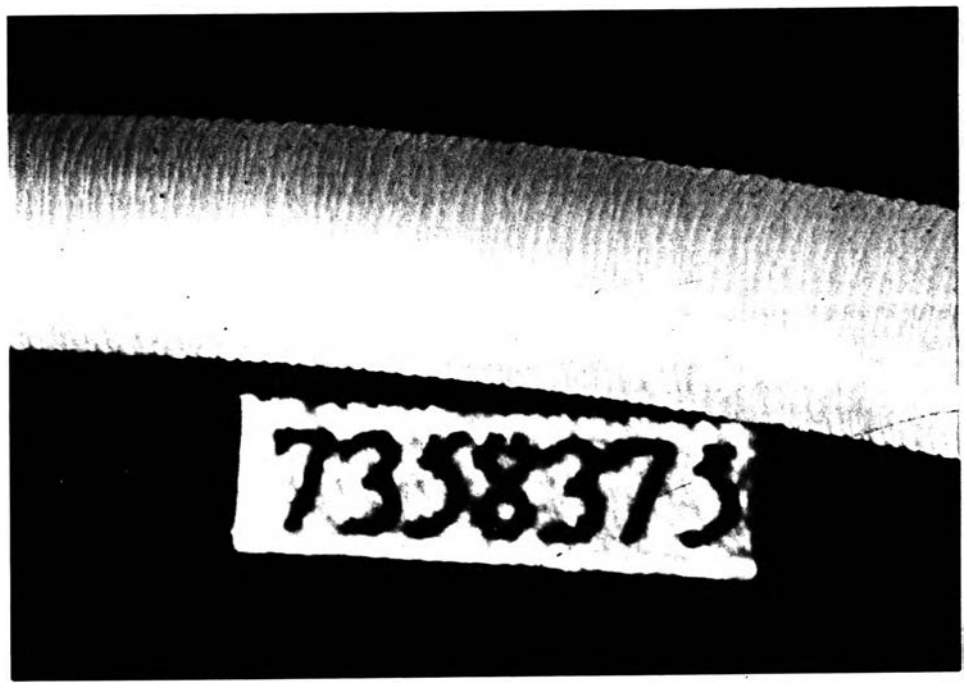

Figure 3.20 Stereomicroscope photograph of a ripple extrudate at HDPE/PP(P340J) : 70/30. ($\gamma \cdot_a$ = 2032 1/sec)

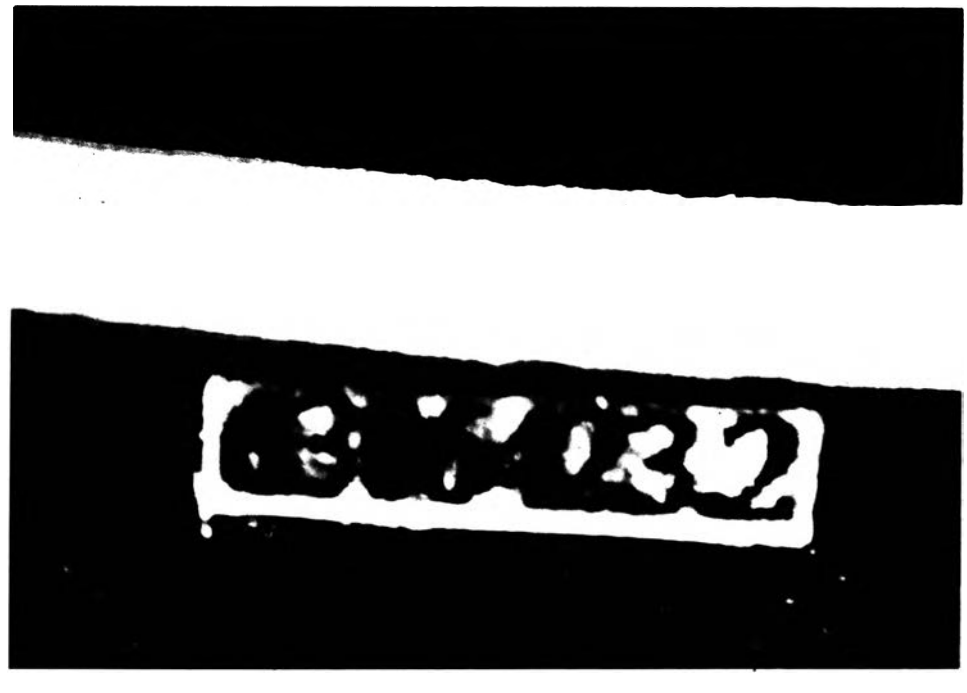

Figure 3.21 Stereomicroscope photograph of a small scale roughness extrudate at HDPE/PP(P340J) : 60/40. ($\gamma \cdot_a$ = 628.5 1/sec)

Figure 3.22 Stereomicroscope photograph of a helix extrudate at HDPE/PP(P340J) : 30/70. ($\gamma \cdot_a$ = 1626 1/sec)

Figure 3.23a Stereomicroscope photograph of a ripple/hazy smooth extrudate in the oscillating regime at HDPE/PP(P340J) : 70/30. ($\gamma \cdot_a$ = 539.1 1/sec)

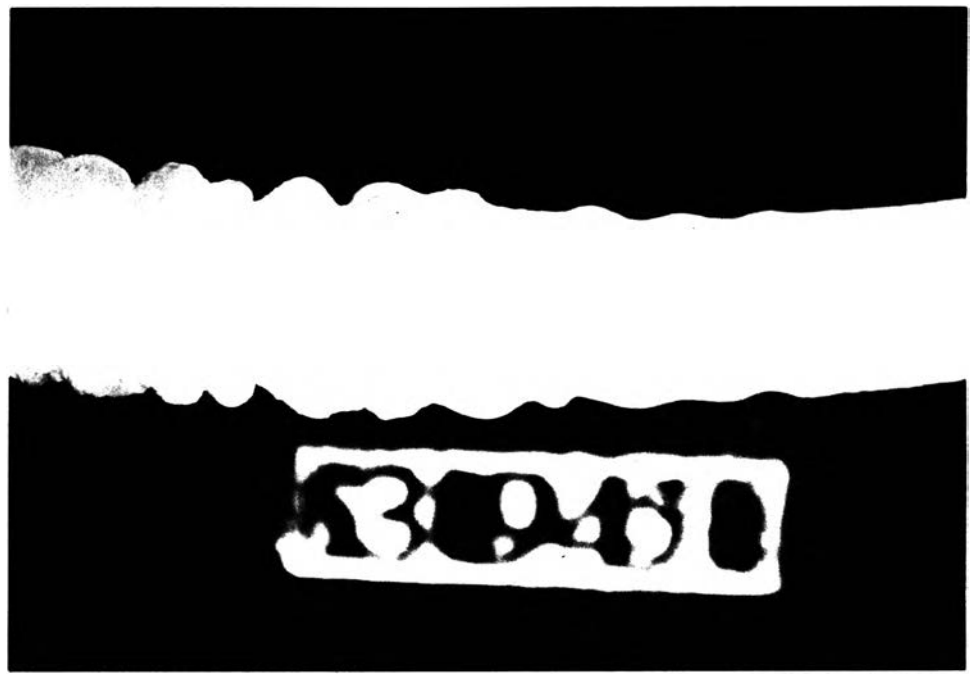

Figure 23b Stereomicroscope photograph of a melt fracture/glossy smooth extrudate in the oscillating regime at HDPE/PP(P340J) : 60/40. ($\gamma \cdot_a$ = 1355 1/sec)

Other observations on the effect of adding PP content were noted from Table 3.2.1. In regime II, as more PP is added the first skin appearance changes from a sharkskin to a peeled orange or the short wavelength instability becomes less favorable than the long wavelength instability. The reason for this phenomenon is not clear to us. But it seems to be a well known fact that a sharkskin or a peeled orange does not occur with every materials, therefore their instabilities should be material dependent whose nature requires further investigation. Similar behaviors were observed in regime III where we found that the skin texture changes from a sharkskin to a ripple to a melt fracture as more PP is added. The progressive effect of PP content is illustrated in Figure 3.24.

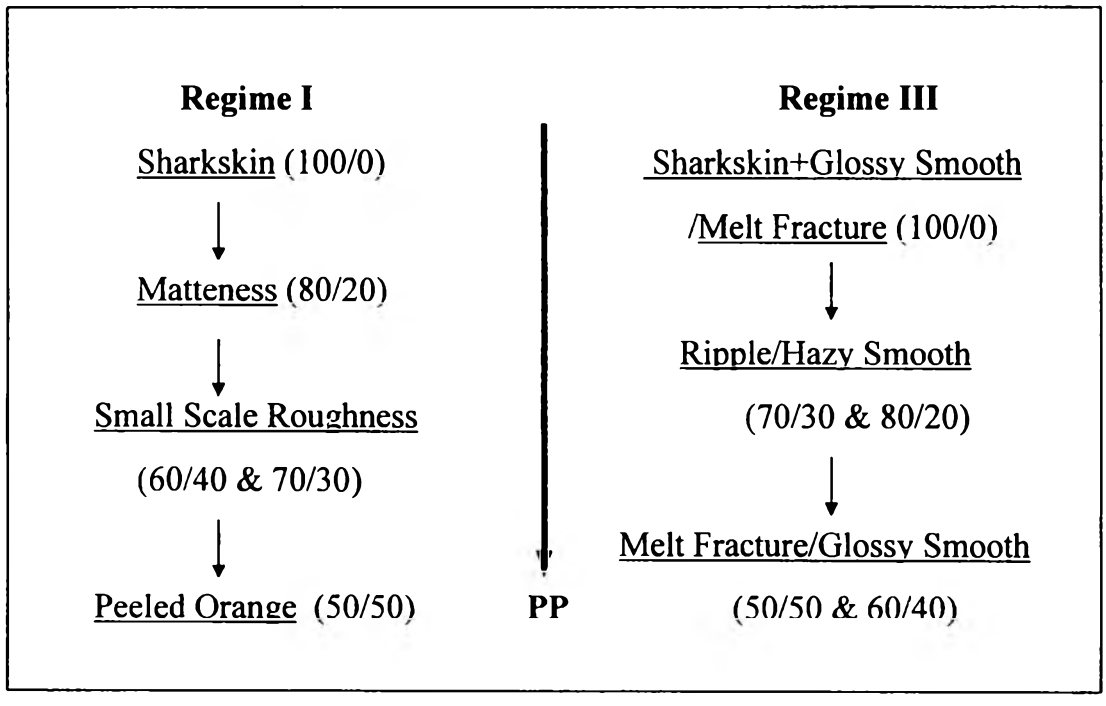

Figure 3.24 Progressive effect of PP content on the blend skin textures.

Table 3.2.1 Surface Textures of HDPE/PP blends

Regime	Surface Texture	HDPE/PP (P340J)									HDPE/PP (P400S)
		100/0	80/20	70/30	60/40	50/50	40/60	30/70	20/80	0/100	70/30
I	**Smooth** **- Glossy Smooth** **- Hazy Smooth**	**	**	**	**	**	**	**	**	**	**
II	**Sharskin**	** $\gamma'_{a,c}$ = 8.66E+01 $\tau_{w,c}$ = 2.05E+05									
	Matteness		** $\gamma'_{a,c}$ = 3.41E+02 $\tau_{w,c}$ = 3.15E+05								
	Small Scale Roughness			** $\gamma'_{a,c}$ = 1.25E+02 $\tau_{w,c}$ = 1.82E+05	** $\gamma'_{a,c}$ = 6.28E+02 $\tau_{w,c}$ = 3.07E+05						** $\gamma'_{a,c}$ = 3.09E+02 $\tau_{w,c}$ = 2.14E+05
	Peeled Orange					** $\gamma'_{a,c}$ = 1.27E+03 $\tau_{w,c}$ = 3.18E+05	** $\gamma'_{a,c}$ = 1.27E+03 $\tau_{w,c}$ = 2.79E+05			** $\gamma'_{a,c}$ = 1.31E+03 $\tau_{w,c}$ = 2.17E+05	
	Helix							** $\gamma'_{a,c}$ = 1.42E+03 $\tau_{w,c}$ = 2.94E+05	** $\gamma'_{a,c}$ = 1.62E+03 $\tau_{w,c}$ = 3.02E+05		

cont.

Regime	Surface Texture	HDPE/PP (P340J)									HDPE/PP (P400S)
		100/0	80/20	70/30	60/40	50/50	40/60	30/70	20/80	0/100	70/30
III	**Oscillation**										
	- Sharkskin+ Glossy Smooth / Melt Fracture	** $\dot{\gamma}_{a,c}$ = 2.98E+02 $\tau_{w,c}$ = 3.36E+05									
	- Ripple/ Hazy Smooth		** $\dot{\gamma}_{a,c}$ = 4.52E+02 $\tau_{w,c}$ = 3.53E+05	** $\dot{\gamma}_{a,c}$ = 5.36E+02 $\tau_{w,c}$ = 3.35E+05							
	- Melt Fracture/ Glossy Smooth				** $\dot{\gamma}_{a,c}$ = 8.10E+02 $\tau_{w,c}$ = 3.31E+05	** $\dot{\gamma}_{a,c}$ = 1.65E+03 $\tau_{w,c}$ = 3.29E+05					** $\dot{\gamma}_{a,c}$ = 7.78E+02 $\tau_{w,c}$ = 3.16E+05
	Helix						** $\dot{\gamma}_{a,c}$ = 1.70E+03 $\tau_{w,c}$ = 3.33E+05				
	Melt Fracture							** $\dot{\gamma}_{a,c}$ = 1.93E+03 $\tau_{w,c}$ = 3.22E+05	** $\dot{\gamma}_{a,c}$ = 1.86E+03 $\tau_{w,c}$ = 3.33E+05		

cont.

Regime	Surface Texture	HDPE/PP (P340J)									HDPE/PP (P400S)
		100/0	80/20	70/30	60/40	50/50	40/60	30/70	20/80	0/100	70/30
IV	**Peeled Orange**	** $\dot{\gamma}_{a,c}$ = 1.48E+03 $\tau_{w,c}$ = 2.75E+05									
	Ripple		** $\dot{\gamma}_{a,c}$ = 1.53E+03 $\tau_{w,c}$ = 2.97E+05	** $\dot{\gamma}_{a,c}$ = 1.68E+03 $\tau_{w,c}$ = 3.01E+05							
	Melt Fracture				** $\dot{\gamma}_{a,c}$ = 1.81E+03 $\tau_{w,c}$ = 2.75E+05	** $\dot{\gamma}_{a,c}$ = 2.31E+03 $\tau_{w,c}$ = 3.05E+05					** $\dot{\gamma}_{a,c}$ = 1.88E+03 $\tau_{w,c}$ = 2.94E+05
	Oscillation - Melt Fracture/ Glossy Smooth						** $\dot{\gamma}_{a,c}$ = 1.80E+03 $\tau_{w,c}$ = 3.37E+05				
V	**Melt Fracture**	** $\dot{\gamma}_{a,c}$ = 2.76E+03 $\tau_{w,c}$ = 3.21E+05	** $\dot{\gamma}_{a,c}$ = 3.72E+03 $\tau_{w,c}$ = 4.31E+05	** $\dot{\gamma}_{a,c}$ = 2.52E+03 $\tau_{w,c}$ = 3.37E+05			** $\dot{\gamma}_{a,c}$ = 2.75E+03 $\tau_{w,c}$ = 3.51E+05				

3.3 Bifurcation Diagram

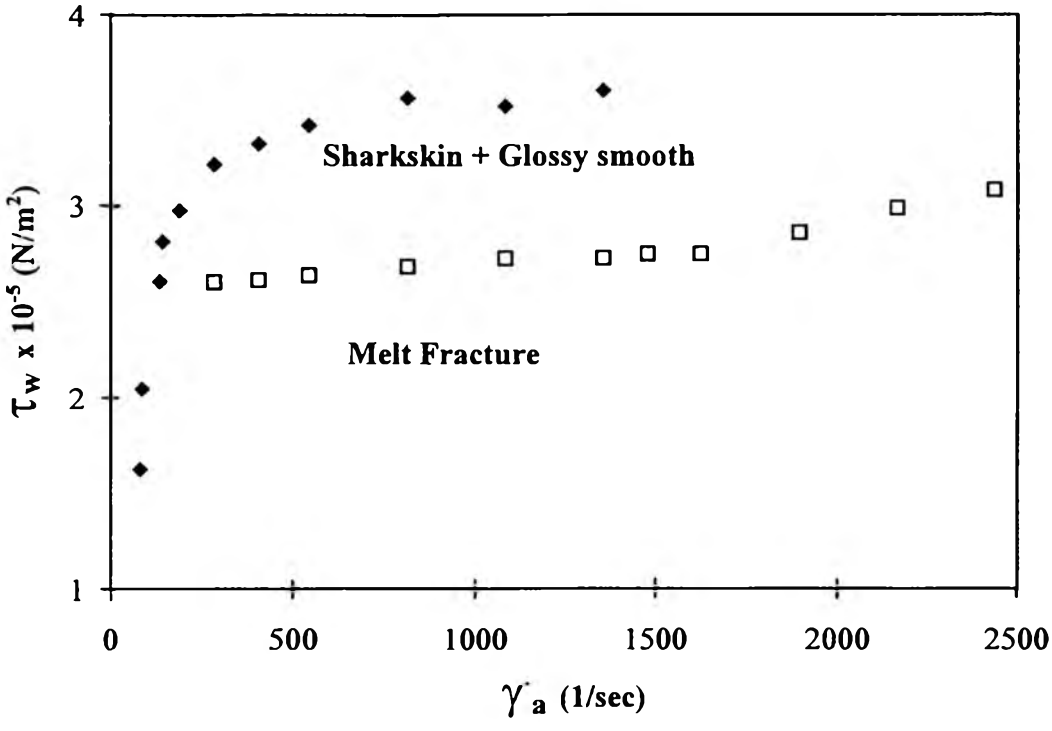

Figure 3.25 Flow curve of HDPE/PP : 100/0 blends.

Figure 3.25 shows the HDPE flow curve in the oscillating regime consisting of upper and lower branches. The upper branch refers to the maximum load in the cycle. Similarly, the lower branch refers to the minimum load in the cycle. The upper branch corresponds to the end of the sharkskin/smooth segment. The lower branch specifies an end of the melt fracture section extrudate. We identify the transition from a steady state to the oscillating regime as a ***Hopf bifurcation***. We note that the steady state flow curve prior to the onset of the bifurcation is continuous with the unstable upper branch. On the other hand, the unstable lower branch prior to the terminal point is continuous with the steady state flow curve beyond the oscillating regime. For the other blends, the flow curves are shown in Figures B.1-B.5 of Appendix B.

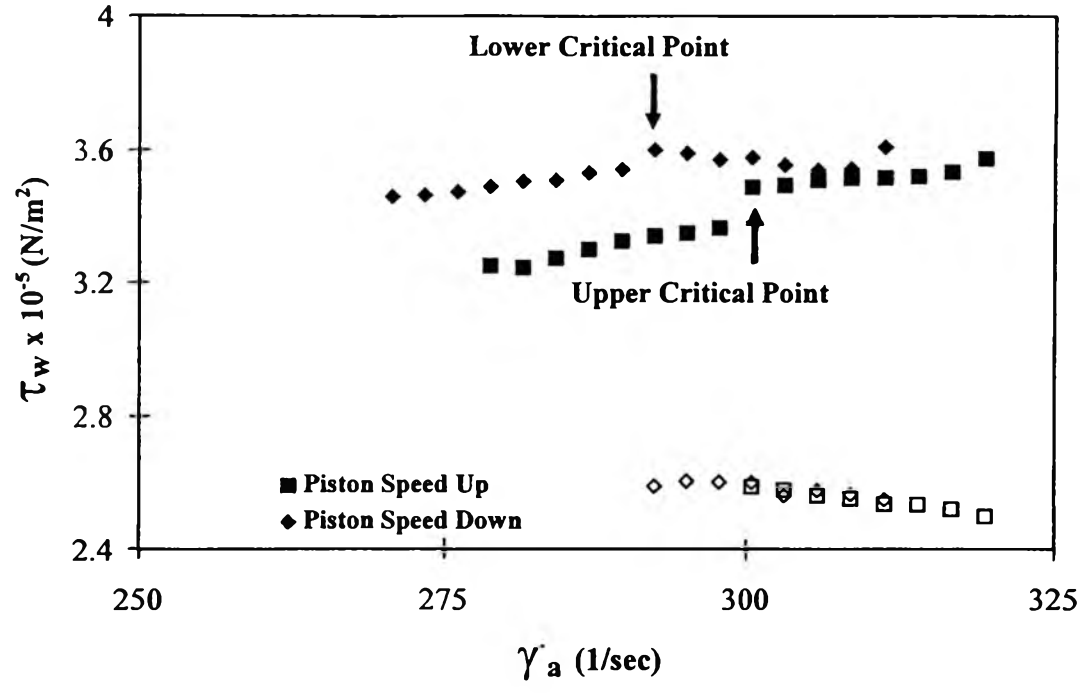

(a)

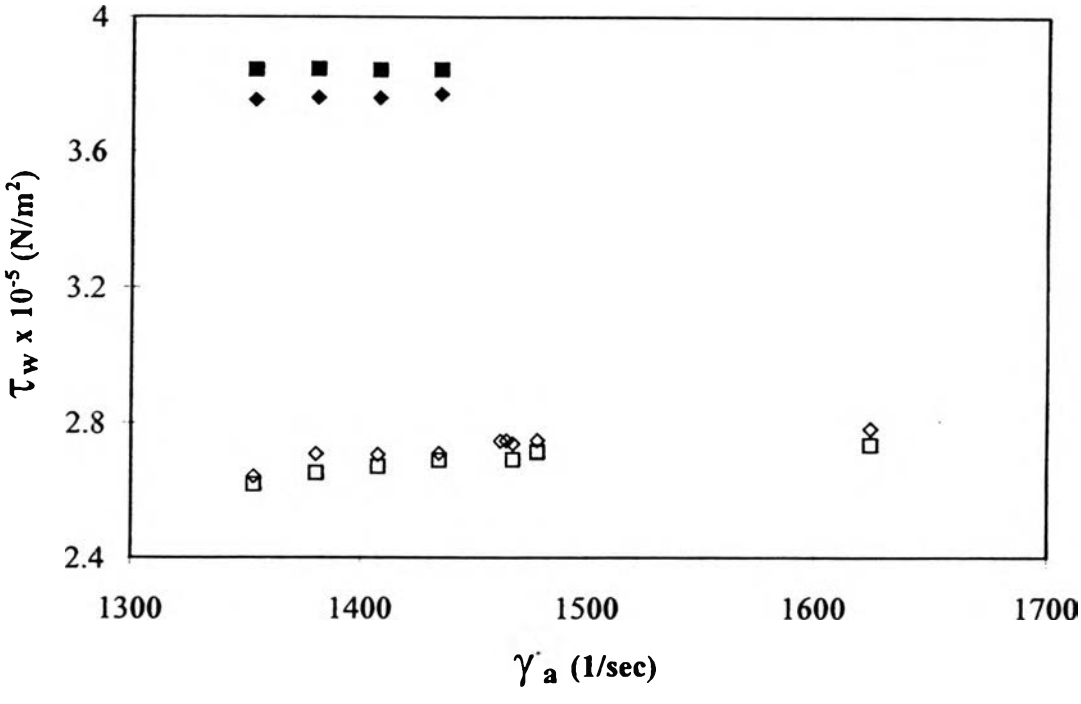

(b)

Figure 3.26 Hysteresis of the bifurcation diagram of HDPE/PP (P340J) : 100/0 in the oscillating regime. (a) The onset of the oscillating regime, (b) The end of the oscillating regime.

A subcritical Hopf bifurcation is normally accompanied by a hysteresis or a path-dependent flow curve. A supercritical Hopf bifurcation is unique and can be identically obtained either when the bifurcation parameter is increased or decreased. In order to test this hypothesis, we carried out two separate experiments for the HDPE. The volume flow rate or the strain rate was increased gradually and we observed an onset of the Hopf bifurcation at a critical apparent strain rate of 297.8 1/s, as shown in Figure 3.26 (a). Upon decreasing the strain rate, we found that the oscillation in the load completely vanished when the strain rate was equal to 289.6 1/s. Therefore the onset depends on whether the volume flow rate is decreased or increased. Similarly, at the terminal point we found that the critical strain rate was 1467 1/s when the volume flow rate was increased and 1462 1/s when the volume flow rate was decreased, as shown in Figure 3.26 (b). We can conclude definitely that the bifurcation points of the oscillating regime are path dependent and thus the bifurcations are ***subcritical***. In addition, we always observed that the jump in stress level between the lower and the upper branches at the onset or at the terminal points were severe; this property is normally associated with a subcritical bifurcation.

3.4 Wavelength

Figures 3.27-3.29 show the load wavelength and the skin wavelength as functions of the apparent strain rate for the three blends studied. The load wavelength was calculated from a period of load oscillation using the incompressibility constraint and the average value of 3-4 measurements was taken. The procedure may be referred to in Appendix A. The skin wavelength was obtained from direct measurements using a ruler with a resolution of 1 mm. The average value was obtained from 3-4 measurements.

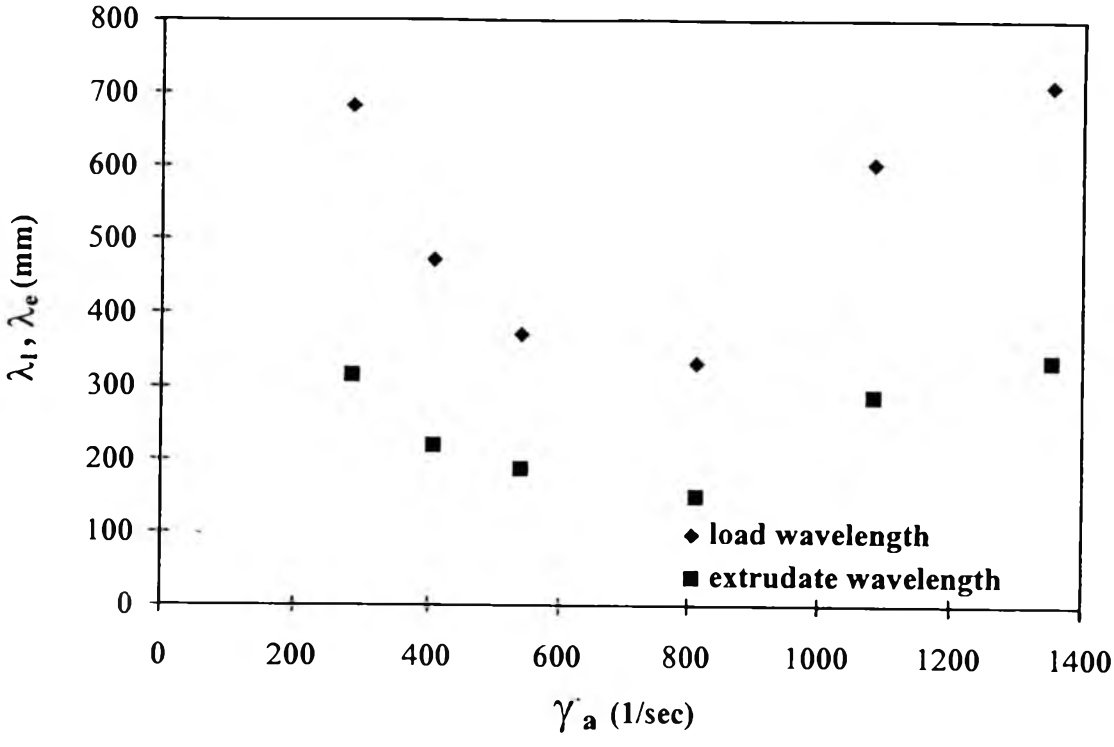

Figure 3.27 The wavelength, λ, versus the apparent strain rate, $\dot{\gamma}_a$, in the oscillating regime of the HDPE/PP : 100/0 blends.

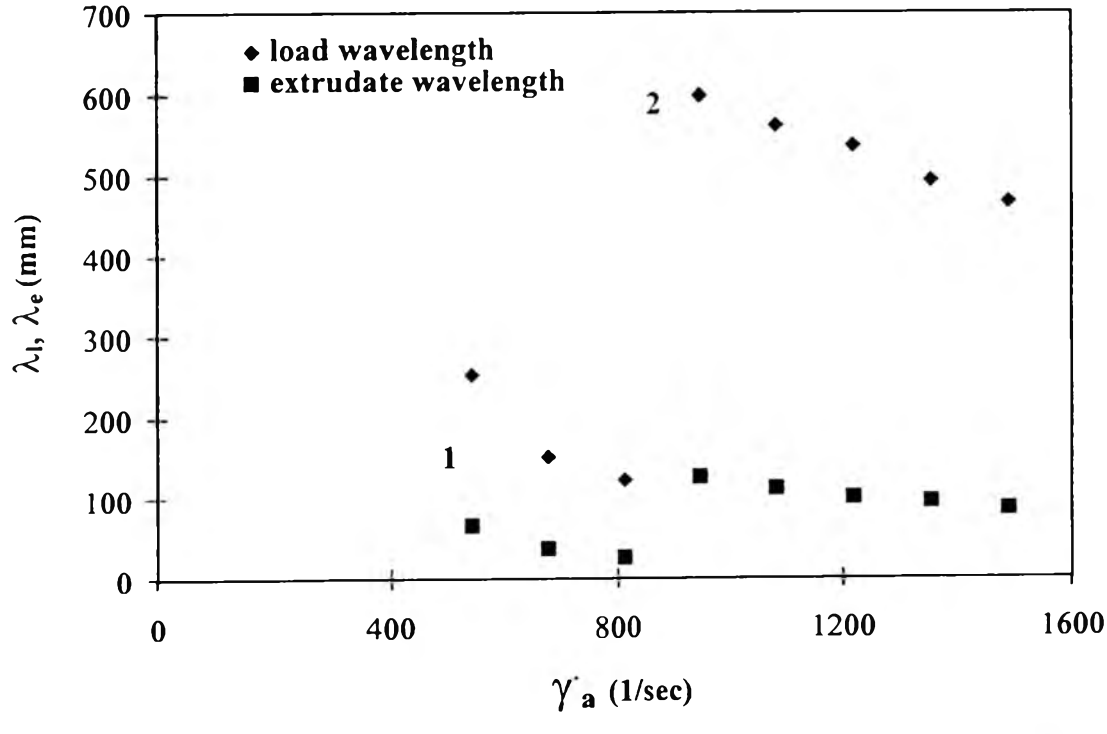

Figure 3.28 The wavelength, λ, versus the apparent strain rate, $\dot{\gamma}_a$, in the oscillating regime of the HDPE/PP : 80/20 blends.

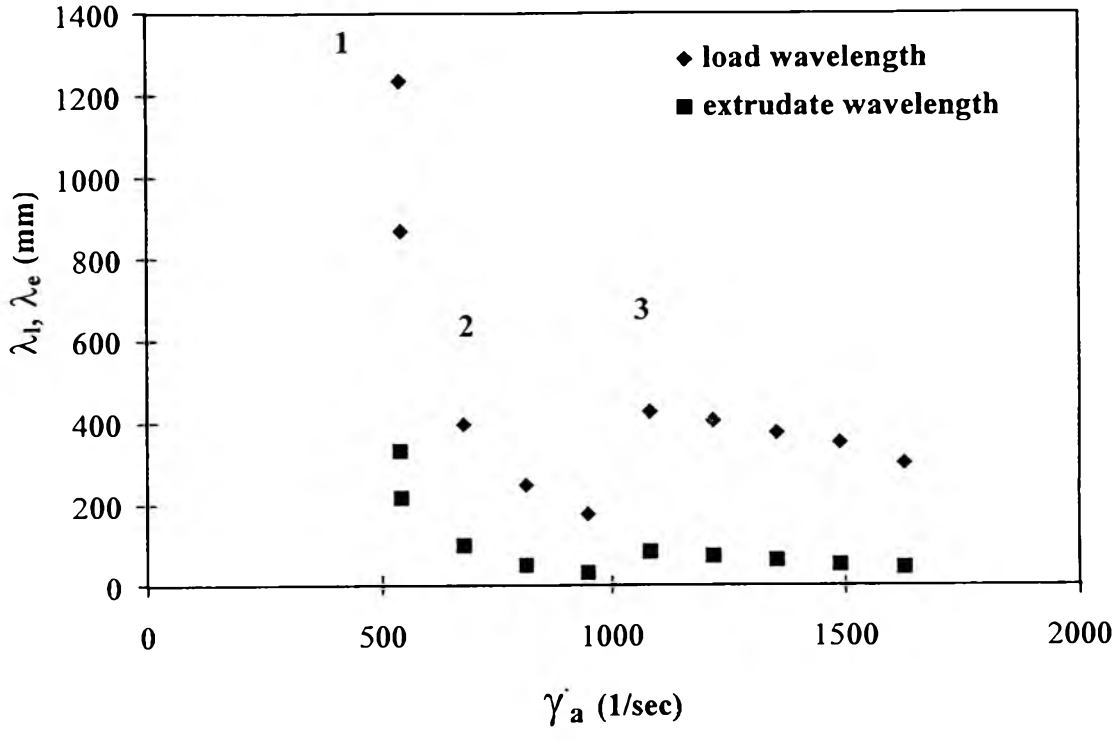

Figure 3.29 The wavelength, λ, versus the apparent strain rate, $\dot{\gamma}_a$, in the oscillating regime of the HDPE/PP : 70/30 blends.

For the HDPE/PP:100/0 blend, we carried out the experiment using only the material from a single barrel. For the HDPE/PP: 80/20 and HDPE/PP: 70/30 blends, we ran a series of experiments using two and three barrels respectively. We see that there are discontinuities in the load and the skin wavelengths at the reloadings of the barrel. This result is consistent with those of Kalika and Denn (1987) who explained that the load wavelength is a strong function of the amount of material remaining in the barrel.

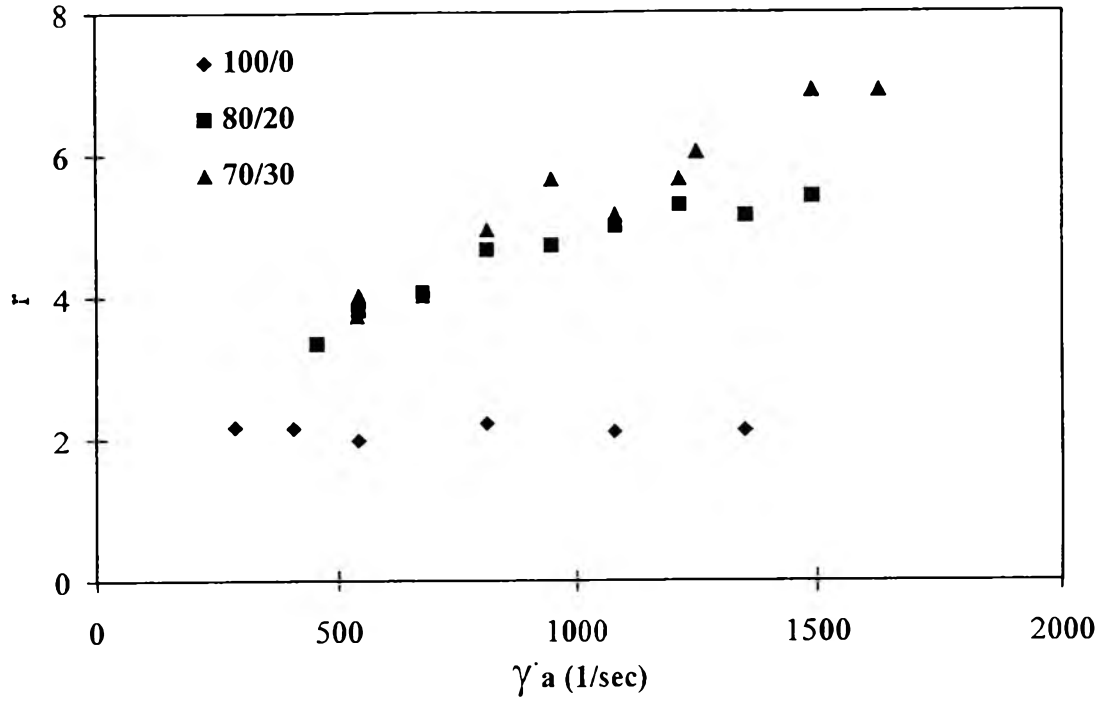

Figure 3.30 The wavelength ratio versus the apparent strain rate, $\dot{\gamma}_a$, in the oscillating regime of the HDPE/PP : 100/0, 80/20 and 70/30 blends.

In Figure 3.30, we plotted the wavelength ratios versus the apparent strain rate of the three blend samples studied. The wavelength ratio is defined as,

$$r = \frac{\lambda_{load}}{\lambda_{skin}} \quad . \tag{3.4}$$

We found that the ratio is larger for a blend with more PP content and it is slightly dependent on the apparent strain rate. We found that the ratio varies between 2-6 , depending on the composition and the strain rate. There are two main reasons why the ratio observed is not close to unity. The load wavelength was calculated assuming that the melt was incompressible but it is commonly accepted that a melt is always compressible. The load wavelength was calculated during the runs at the melt temperature whereas the skin wavelength was obtained when the melt had already solidified to become an extrudate at the room temperature. The difference in temperature can account for the

departure of the wavelength ratio from unity because of the melt free volume depends strongly on temperature.

3.5 Slip Velocity

The slip velocity was calculated only in the oscillating regime for each blend using equation (A.15) in Appendix A. Figure 3.31 shows the average slip velocity, V_S , versus the apparent strain rate corrected for slip, $\gamma_{a,S}$, for all our blend samples. Each average value was taken from 3-4 measurements. Standard deviations of the slip velocity measurements can be found in Appendix B.

In Figure 3.31, we find that the slip velocity varies linearly with the apparent strain rate corrected for slip for all our blend samples. However, the dependence of V_S on $\gamma_{a,S}$ can be classified into two cases. In one case of HDPE-riched blends,

$$V_s = C_1 \gamma^{\circ}_{a,s} \quad , \tag{3.5a}$$

where C_1 is a composition dependent constant. Here, the slip can occur even in the limit of low strain rate. In this case, disentanglement takes place continuously in the molecular layer at the melt/wall interface. It mean that the polymer chain can slide pass through a capillary and a slip layer always exist even in the limit of a small strain rate.

In the other case of PP-riched blends,

$$V_s = C_0 + C_1 \gamma^{\circ}_{a,s} \quad , \tag{3.5b}$$

where C_0 is a negative constant and C_1 is a composition dependent constant. Here, the slip can occur only if the apparent strain rate or the wall shear stress is sufficiently large. In this case the disentanglement is quite abrupt and a test polymer chain finds itself more difficult to reptate in an environment

consisting of more chains of another specie, as is the case when more PP is added.

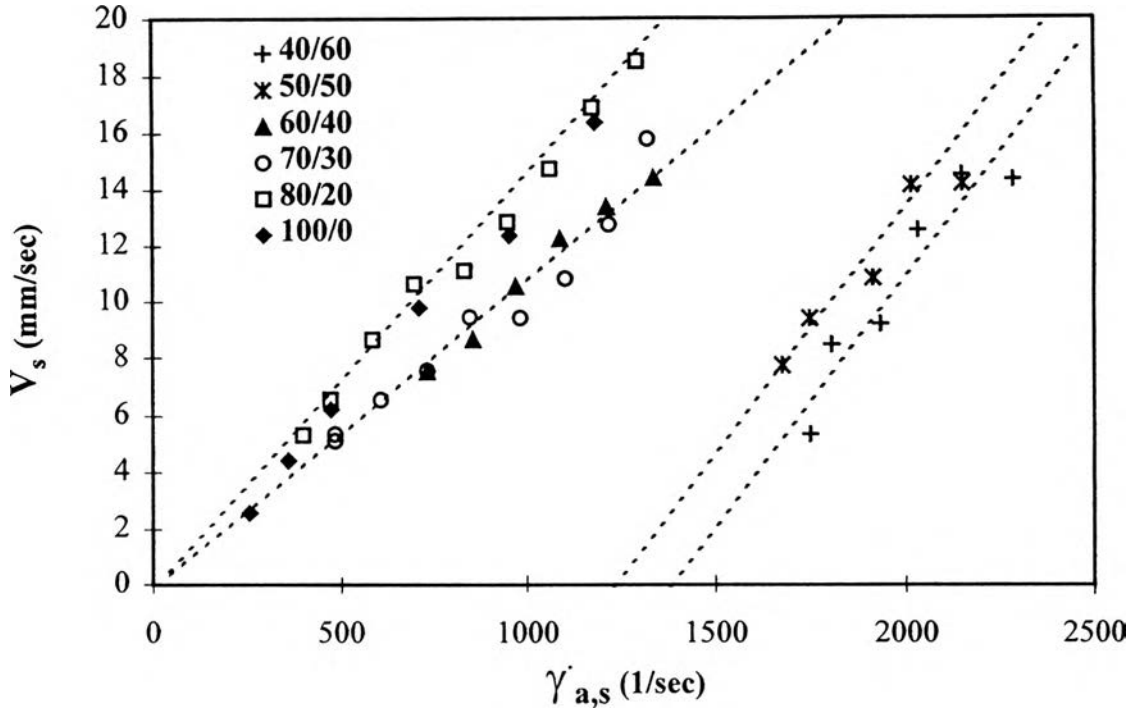

Figure 3.31 The slip velocity, V_S, versus the apparent wall strain rate corrected for slip, $\dot{\gamma}_{a,S}$, in the oscillating regime.

3.6 The Extrapolation Length

Figure 3.32 shows the extrapolation length, b, versus the apparent strain rate corrected for slip, $\dot{\gamma}_{a,s}$, in the oscillating regime. The extrapolation length was calculated from equation (A.17) in Appendix A.

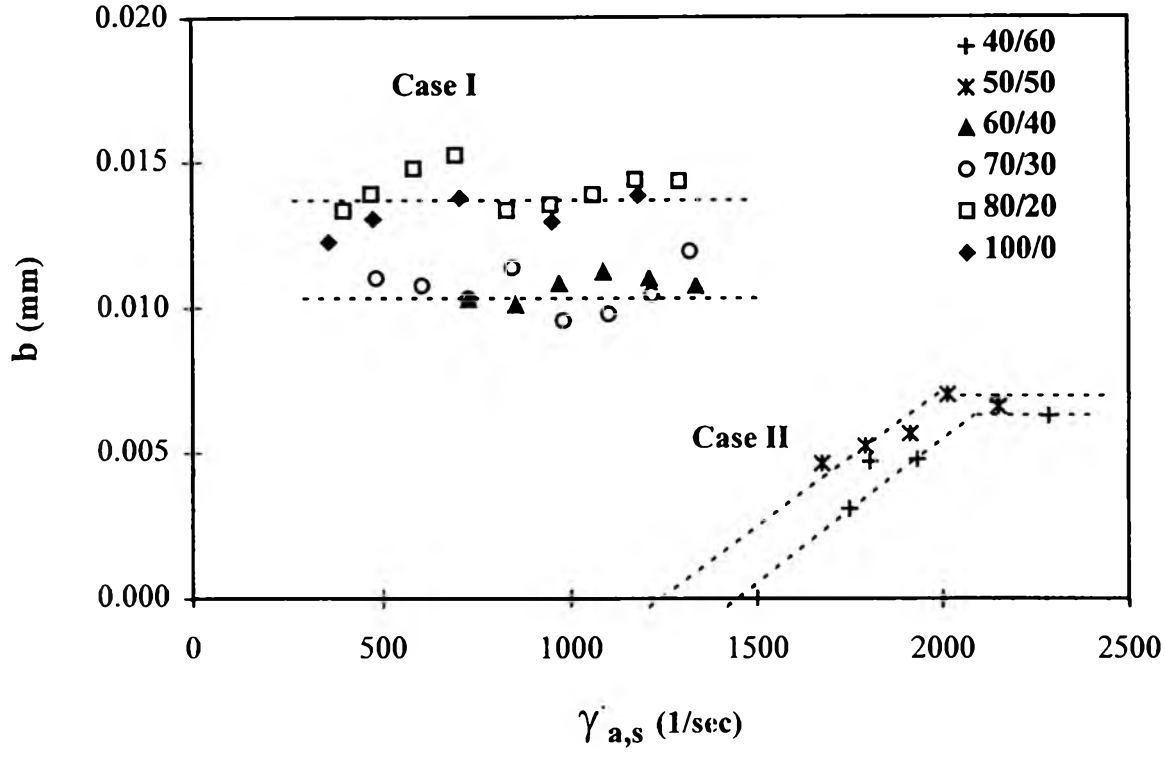

Figure 3.32 The extrapolation length, b, versus the apparent wall strain rate corrected for slip, $\dot{\gamma}_{a,s}$, for HDPE/PP (P340J) blends in the oscillating regime.

We found that there are essentially two cases. The extrapolation length of the HDPE-riched blends seems to be independent of the strain rate, whereas that of the PP-riched blends varies with the strain rate initially until reaching their asymptotic values at high strain rates. The results here are consistent with equations (3.5a) and (3.5b) where we can write for the latter equation,

$$b = \frac{C_0}{\dot{\gamma}_{a,s}} + C_1 . \qquad (3.6a)$$

In the first case, the extrapolation length is a constant and independent of the apparent strain rate and its value is C_1 of equation (3.5a). C_1 is not a universal constant but it depends on PP content For the PP-riched blends or the second case, b asymptotes to C_1 of equation (3.5b) in the limit of a large strain rate. The constant C_1 depends slightly on the PP content. It seems that an addition of PP content into a blend delays a continuous disentanglement. Above a certain level of PP, a certain stress level is required to initiate a disentanglement at the interface and the reptation motion is hindered resulting in a lower value of the extrapolation length. This result is possibly due to an effect of the χ_i interaction parameter as well.

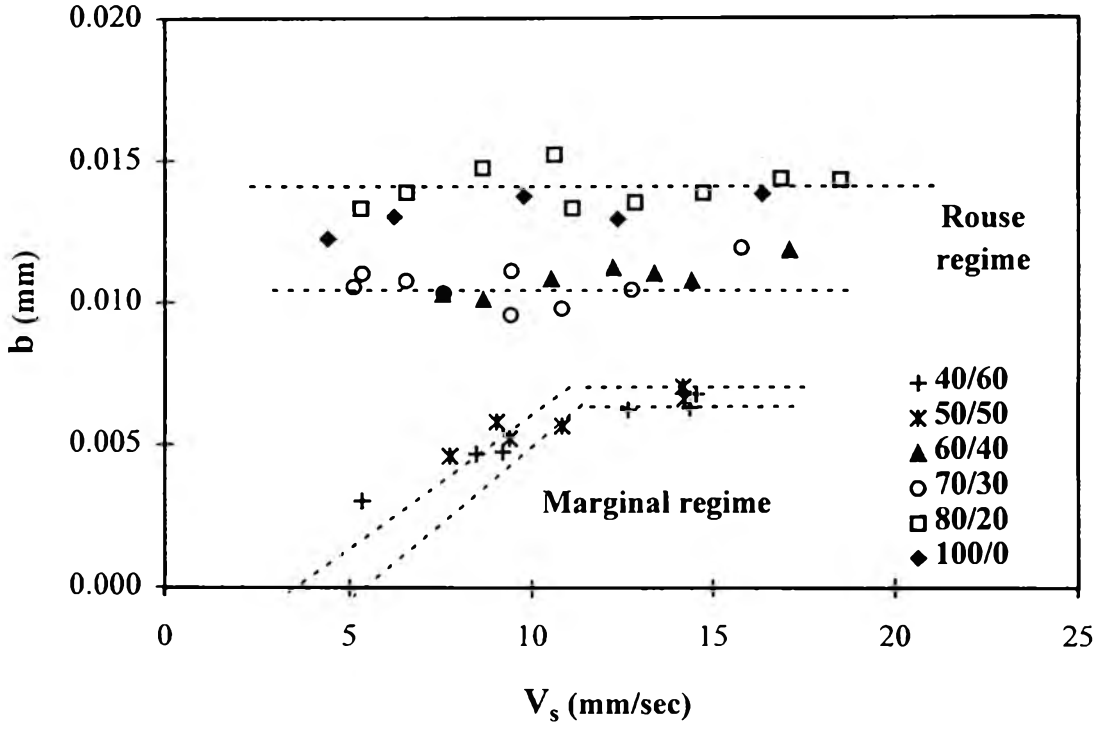

Figure 3.33 The extrapolation length, b, versus the slip velocity, V_S, for HDPE/PP (P340J) blends in the oscillating regime.

Figure 3.33 shows the extrapolation length versus the slip velocity. We found that again the data can be divided into two sets. For the HDPE-riched blends, the extrapolation length is independent of the slip velocity and hence the slippage is referred to as the Rouse regime (Brochard and de Gennes 1992). For the PP-riched blends, the extrapolation length varies with the strain rate until reaching its asymptotic value. The slippage for the latter system is possibly in the Marginal regime as predicted by Brochard and de Gennes. The difference between the two systems or the two regimes are: the marginal state refers to the state of melt chains which have been completely extended and the extrapolation length is a linear function of slip velocity. The Rouse regime is correlated with the situation where the slippage length is independent of the slip velocity since the chains can reptate freely.

3.6.1 Effect of Composition

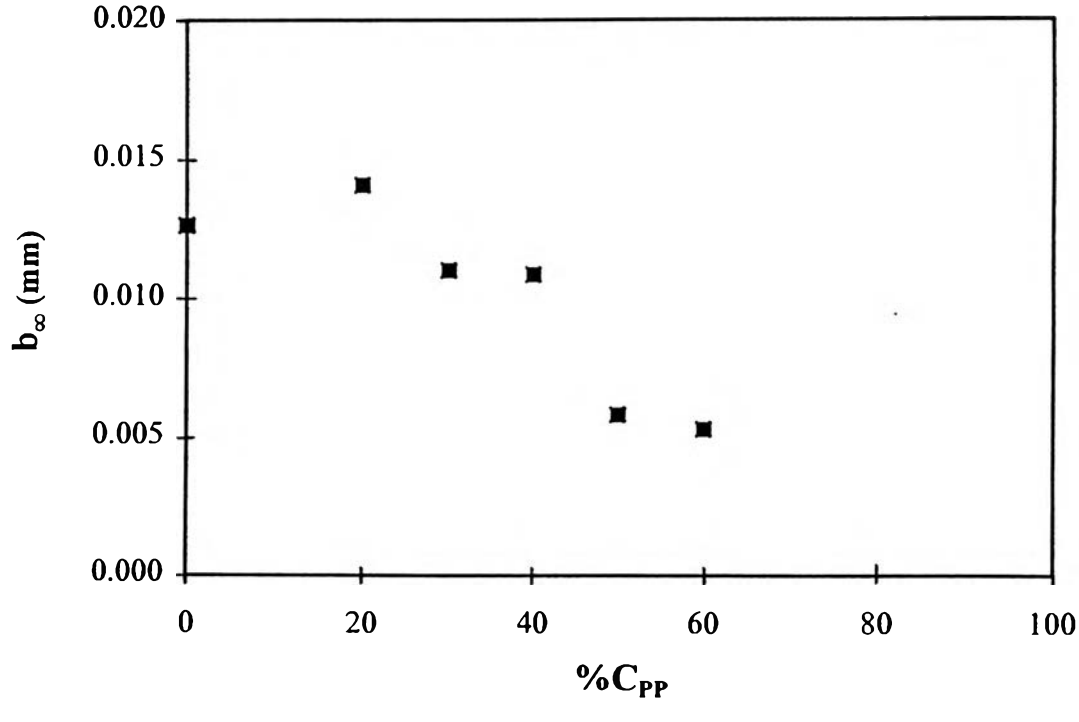

Figure 3.34 Composition effect on the asymptotic extrapolation length, b_∞ ,for HDPE/PP (P340J) blends.

Figure 3.34 shows the asymptotic extrapolation length as a function of PP content. We found that the extrapolation length indeed varies with PP content. It decreases from the value of 0.013 mm to the value of 0.005 mm as the PP content was varied form 0 to 60 %. For pure HDPE, disentanglement was smooth and the polymer chains can easily reptate amongst their own type as the χ_i interaction parameter is null. For the PP-riched blends, disentaglement occurs abruptly and only when the strain rate or the wall shear stress is above its critical value. Our result suggests that disentanglement can be delayed and that the reptation motion is hindered when a test chain has to reptate in an environment consisting of other chains of different species or when the χ_i parameter is different from zero.

3.6.2 Effect of Melt Flow Index

Table 3.6.1 shows the asymptotic extrapolation lengths for two blends with an identical composition but different melt flow indices. The PP's were of different grade but their molecular weights were nearly the same. We find that for this pair of blends when the melt flow index is twice as large, the asymptotic extrapolation length is reduced by a factor of two. This result may be fortuitous but it seems to support the disentanglement picture that we have used to explain our results.

Table 3.6.1 The asymptotic extrapolation length for each ratio

Material (70/30 ratio)	**M_w of PP (g/mol)**	**MFI (g/10min) 190^{0}C/2.16 kg**	**MFI (g/10min) 230^{0}C/2.16 kg**	**b (mm)**
HDPE/PP (P340J)	174,000	0.538	1.008	0.0146
HDPE/PP (P400S)	176,000	0.997	1.801	0.0071

3.7 Critical Parameters

Critical parameters are the lowest values of the apparent strain rate or the wall shear stress at which a skin texture first appears or the oscillating regime starts to commence. We are concerned with only the appearances of the oscillating regime and the melt fracture texture. Table 3.2.1 summarizes the critical apparent strain rate and the critical wall shear stress for all our blend samples studied.

3.7.1 Effect of composition

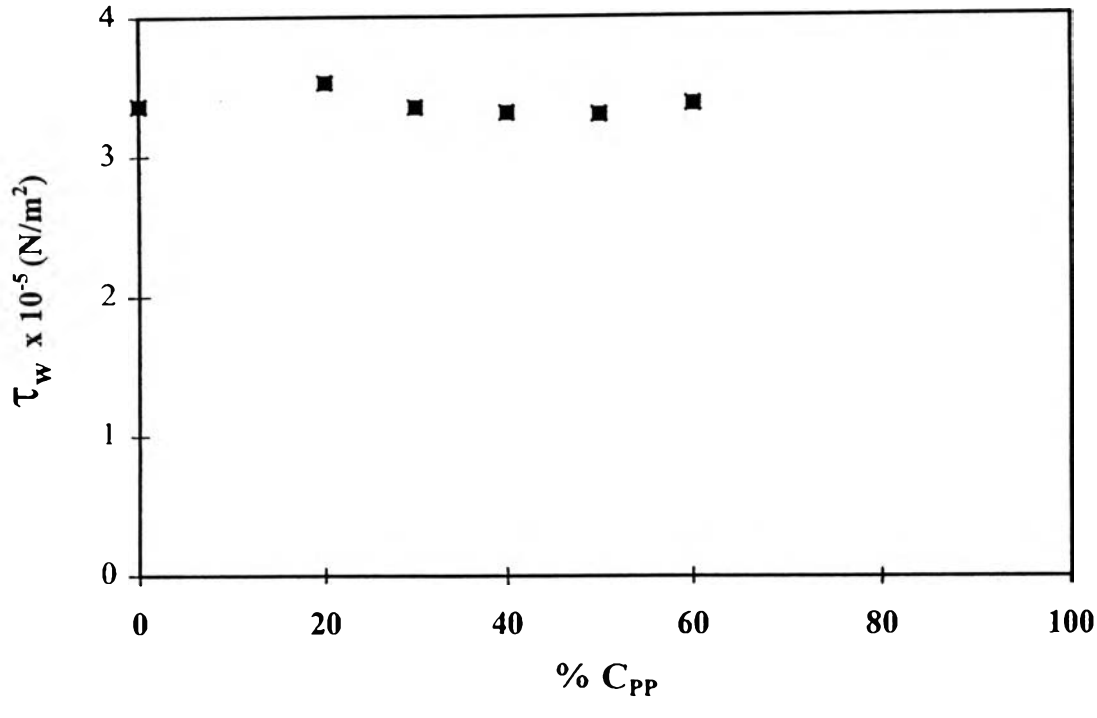

Figure 3.35 Composition effect on the critical wall shear stress, $\tau_{w,c}$, of HDPE/PP (P340J) blends in the oscillating regime.

Figure 3.35 shows the effect of composition of HDPE/PP (P340J) blends on $\tau_{w,c}$ in the oscillating regime. We notice the consistency in the critical wall shear stresses found; they vary between 3.298 -3.528 (10^5 N/m^2) as PP content was varied from 0 to 60 %. This is possibly due to the fact that a certain level of stress is required to initiate chain disentanglement. On the other hand, it is often the case that the stick-slip regime critical wall shear stress is a strong function of molecular weight and temperature (Wang and Drda 1996). In our case, the molecular weights of HDPE and PP are not sufficiently different; they are 100,000 and 170,000 g/mole respectively.

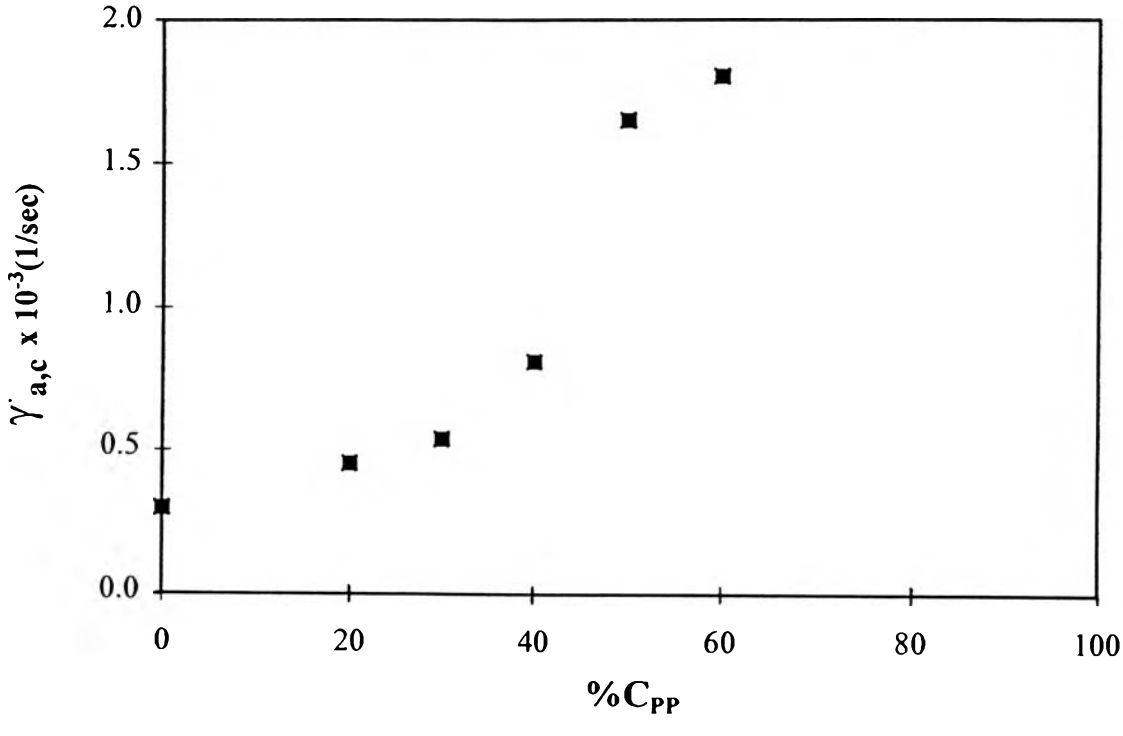

Figure 3.36 Composition effect on the critical apparent strain rate, $\dot{\gamma}_{a,c}$, of HDPE/PP (P340J) blends in the oscillating regime.

Figure 3.36 shows the effect of composition of HDPE/PP blends on the critical strain rate or $\dot{\gamma}_{a,c}$ in the oscillating regime. $\dot{\gamma}_{a,c}$ increases with % PP

content. The main reason for the variation of the critical strain rate is the effect of viscosity; a blend with a large % PP content has a lower viscosity or a larger melt flow index, as illustrated in Table 2.4.1. Another reason may be due to slippage at the capillary surface (Kalika and Denn,1987). PP delayed the slip at the wall as apparent from the increase in the critical strain rate; this implies a hindering of the initiation of disentanglement. The result here is consistent with the slip velocity shown in Figure 3.25.

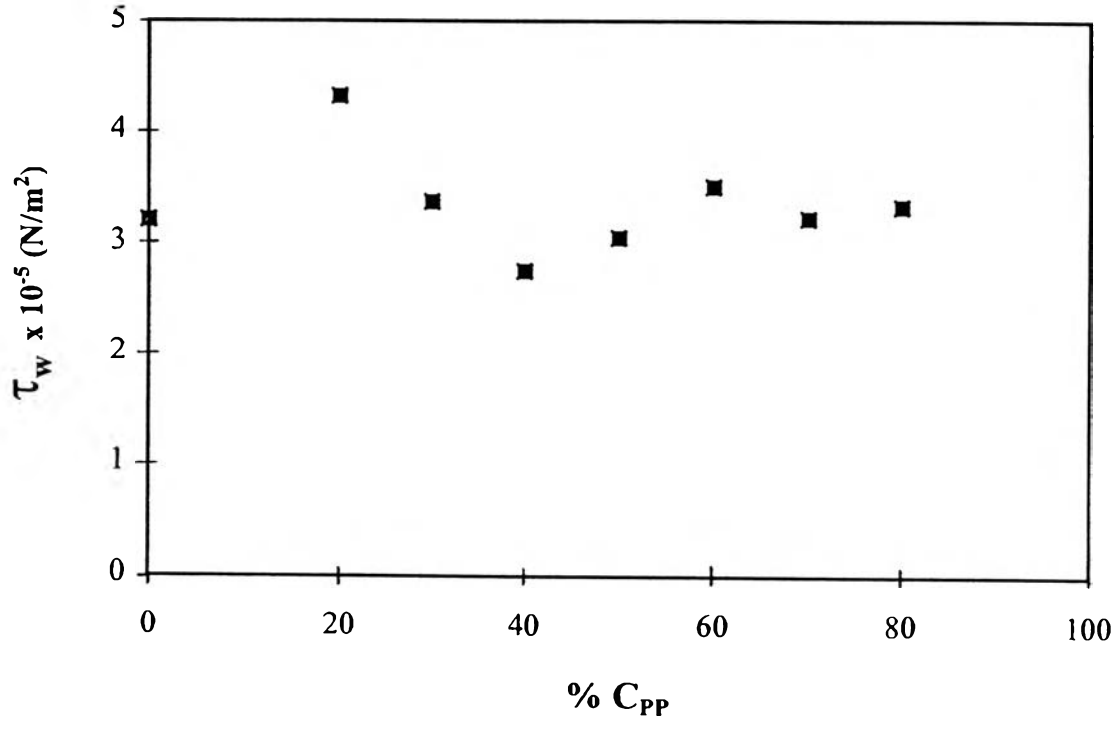

Figure 3.37 Composition effect on the critical wall shear stress, $\tau_{w,c}$, of HDPE/PP (P340J) blends in the melt fracture regime.

Figure 3.37 shows the effect of composition of HDPE/PP blends on the critical wall shear stress of the melt fracture skin. We can observe that the critical wall shear stress hardly varies with the % PP content. It varies between 2.75 - 4.31 (10^5 N/m^2). We can see that the critical wall shear stress does not show a definite trend with the increase of PP content. The immiscible effect

and poor interaction/ or distribution of PP content were thought to be the main cause of the scatters in the data. The other reason is the error made in observation of the onset of the melt fracture. The onset of the melt fracture is difficult to observe than that of the oscillation regime which can be identified from the plunger load.

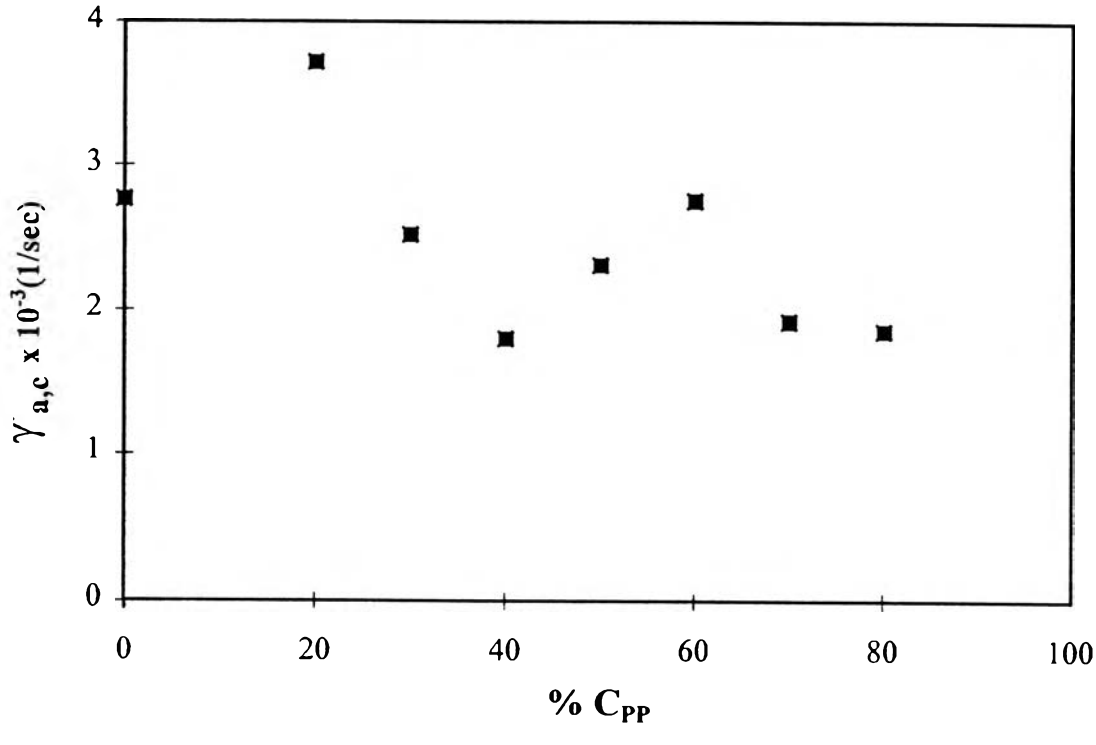

Figure 3.38 Composition effect on the critical apparent strain rate, $\gamma_{a,c}$, of HDPE/PP (P340J) blends in the melt fracture regime.

Figure 3.38 shows the effect of composition of HDPE/PP blends on the apparent critical strain rate. We can observe that the apparent critical strain rate seems to vary with the % PP content. As PP content increases, the critical apparent strain rate decreases. Kalika and Denn (1987) stated that the extrudate distortions of melt fracture skin were caused by the slip at capillary surface. Thus the decrease of the critical strain rate can be explained by the slip at the

wall. PP content exposed at the melt surface can act like ball bearings. This means that the slippage of the melt fracture surface occurs easier for a blend with more PP. So the more content of PP, the lower strain rate the extrudate distortion can occur.

3.7.2 Effect of Melt Flow Index

Table 3.7.1 lists the critical wall shear stresses and the critical apparent strain rates for the oscillating regime and the melt fracture skin. The blends are HDPE/PP (P340J) and HDPE/PP (P400S) at the same composition of 70/30. We see immediately that the critical wall shear stresses for both blends are nearly identical despite the fact that the melt flow index was varied by nearly a factor of two. The main reason is due to the fact that both blends have nearly the same molecular weights and distributions; the difference in the melt flow index stems from commercial additives which play no measurable role in the initiation of disentanglement

Table 3.7.1 The critical parameters for each melt flow index in the oscillating regime

Materials (70/30) ratio	**MFI (g/10min) 190^{0}C/2.16 kg**	**MFI (g/10min) 230^{0}C/2.16 kg**	$\tau_{w,c}$ **(N/m^2)**	$\gamma_{a,c}$ **(1/sec)**
HDPE/PP(P340J)				
Oscillation	0.538	1.008	3.349E+05	5.364E+02
Melt Fracture			3.372E+05	2.520E+03
HDPE/PP(P400S)				
Oscillation	0.997	1.801	3.163E+05	7.775E+02
Melt Fracture			2.944E+05	1.883E+03

3.8 Normalizations

The normalization of the wall shear stress was by the recoverable shear, S_R. S_R is defined as

$$S_R = \frac{\tau_w}{G'} , \qquad (3.8a)$$

where τ_W is the wall shear stress and G′ is shear modulus of the melt. Figure 3.39 shows the time and temperature superposition of the master cure of G′ of pure HDPE.

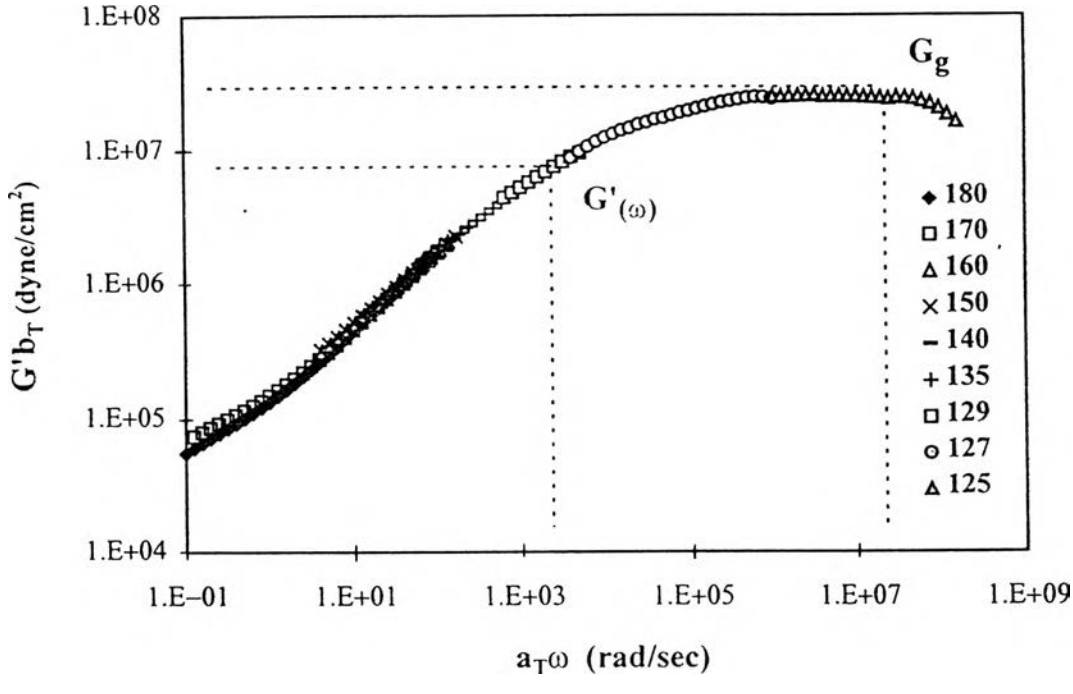

Figure 3.39 The master curve of HDPE/PP (P340J) : 100/0.

In our study, we used the storage modulus (G′) to represent the shear modulus and obtained the value of S_R by two normalizations. The first method used the asymptotic value of G′ which is obtained from the limit of G′ (ω)

as $\omega \rightarrow \infty$ or G_g. Asymptotic normalization is done by setting G′ in equation (3.8a) equal to G_g or the glassy storage modulus :

$$S_R = \frac{\tau_w}{G_g} , \qquad (3.8b)$$

where G_g is determined from master curves of G′ at the melt flow temperature. The master curves were derived from measurements of G′ as a function of the frequency at various temperatures. The principle of the time and temperature superposition was applied to shift G′ curves at different temperatures to form a single master curve at a fixed reference temperature which was the same as the melt flow temperature. The second method, a local value of G′ (ω) was obtained at the frequency corresponding to the critical strain rate of the surface texture. It was done by setting G′ in equation (3.8a) equal to G′ (ω) where ω is

$$\omega = 2\pi\gamma^{\circ}_{a,c}\frac{h}{R} , \qquad (3.8c)$$

where ω is the angular frequency of G′ derived from the parallel plates rheometer, $\gamma^{\circ}_{a,c}$ is the critical apparent strain rate of the extrudate distortion (the oscillation and the melt fracture) h is the gap spacing and R is the radius of plate. The recoverable shear is shown in Tables 3.8.1-3.8.2.

Table 3.8.1 The recoverable shear of HDPE/PP (P340J) : 100/0

Regimes	**$G'b_T$ ($dyne/cm^2$) (Local)**	**G_gb_T ($dyne/cm^2$) (Asymptotic)**	**S_R (Local)**	**S_R (Asymptotic)**
Oscillation	2.40E+06	2.51E+07	1.400	0.133
Melt Fracture	6.87E+06	2.51E+07	0.466	0.127

From Table 3.8.1, we found that S_R obtained from the asymptotic method has a lower value because G_g is of higher value in the glassy state which reflects the stiff chain mobility. Furthermore, S_R for the melt fracture are lower than S_R for the oscillating regime. This is possibly due to the onset of the melt fracture is on the lower branch, and the onset of the oscillation regime is on the unstable upper branch.

In figures B.6-B.12 of Appendix B, we obtained S_R was obtained by the asymptotic method. The chosen temperature was a temperature that G′ begin to form a plateau region without time-temperature superposition. The results are shown in Table 3.8.2; S_R of two regimes were not much different. Except the blend of ratio 50/50 has a higher S_R value possibly of the blend might not be well mixed. We expect that S_R (local) would be closer to order one with a smaller variation, for skin defects whose origins are of cohesive nature.

Table 3.8.2 The recoverable shear (Asymptotic Values)

HDPE/PP (P340J) ratio	**$G_g b_T$ (dyne/cm^2) (Asymptotic)**	**S_R (Oscillating)**	**S_R (Melt Fracture)**
0/100	2.15E+07	-	-
20/80	3.53E+07	-	0.094
30/70	2.66E+07	-	0.121
40/60	2.52E+07	0.134	0.139
50/50	1.46E+07	0.226	0.209
60/40	3.33E+07	0.099	0.083
70/30	2.42E+07	0.138	0.139
80/20	3.57E+07	0.098	0.121
100/0	2.51E+07	0.134	0.127

3.9 Viscosity

3.9.1 Steady State vs. Oscillatory State

We now compare the viscosities obtained from the capillary and the parallel plate rheometers. The capillary rheometer gives a steady state viscosity as a function of steady state strain rate, whereas the parallel plate rheometer provides us with a complex viscosity as a function of frequency. To compare the two viscosities, we need to convert the frequency in to a representative steady state strain rate. The transformation can be accomplished the following equation,

$$\dot{\gamma}_w = \frac{\omega R}{2\pi h}, \tag{3.9}$$

where ω is frequency or angular velocity, R is radius of the parallel plates and h is gap spacing. We note that the transformation is not exact because the strain rate field of a parallel plate is not homogeneous and it is unsteady as well. So the transformation is both time and space averaging.

Figures 3.40 (a) and 3.41 (a) show the viscosities as functions of the apparent strain rate and the transformed strain rate for HDPE and PP respectively. We can see that for HDPE, both viscosities collapse well at high strain rates but deviations can be clearly seen at low strain rates. The capillary viscosity is lower that the parallel plate viscosity. The reason for this may be due to slippage at the low strain rates in which the slip magnitude is comparable to the actual strain rate. The ratio of slip magnitude to the actual strain rate becomes smaller at the high strain rates and the slip effect becomes more obscure. Other reason may be caused by the inexact transformation of equation (3.9) introduced by us. For PP, the viscosity obtained form the capillary rheometer is always higher than the viscosity obtained from the parallel plate rheometer. This may be caused by the entrance and exit losses which we have

not taken into account in the capillary analysis. We did not apply the Bagley correction.

Cox-Merz rule (1958) equates the magnitude of the complex viscosity to the steady-shear viscosity. It equates the parallel plate complex viscosity (η^*) vs. frequency (ω) to the capillary viscosity (η') vs. the apparent strain rate (γ_a). The results are shown in Figures 3.40 (b) and 3.41 (b). The results of comparing the viscosities using the Cox-Merze rule are the same as the result using our transformation. The physical explanations are therefore assumed to be the same. It is our pleasure to note that our transformation can provide a systematic and semi-quantitative scheme for comparing the steady state viscosity and the oscillatory viscosity.

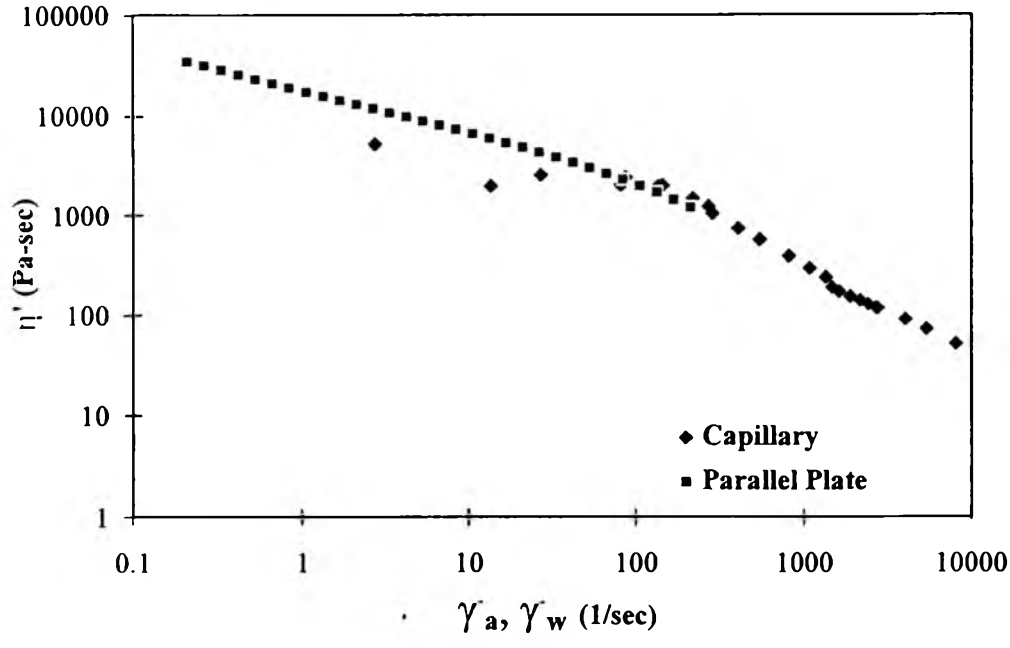

(a)

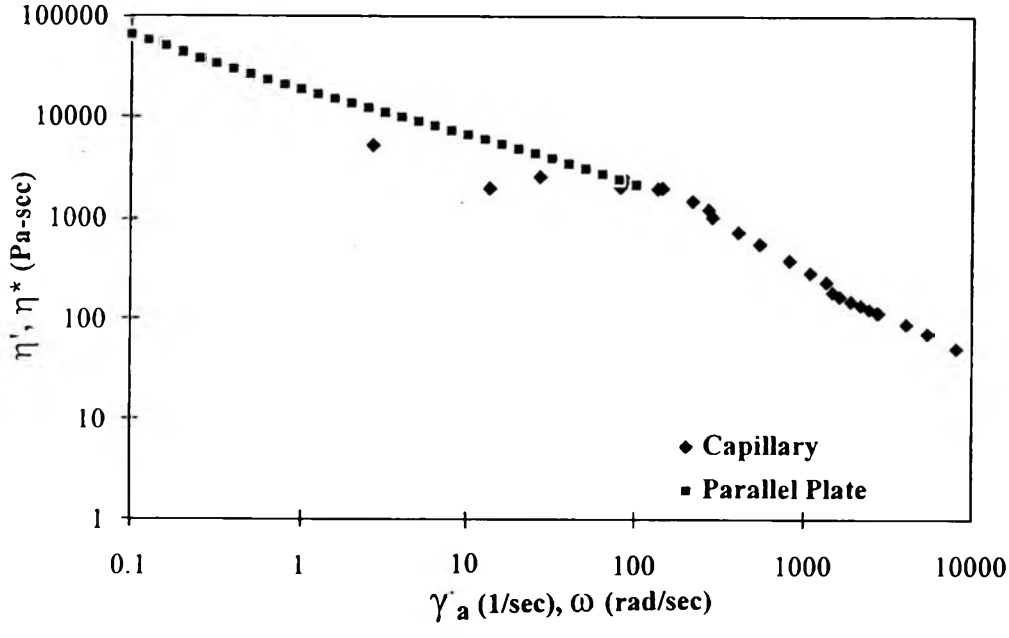

(b)

Figure 3.40 (a) Comparison of the capillary viscosity vs. the apparent strain rate and the parallel plate viscosity vs. the apparent wall strain rate for the HDPE/PP (P340J): 100/0 blends. (b) Comparison of the capillary viscosity vs. the apparent strain rate and the parallel plate complex viscosity vs. the frequency for HDPE/PP (P340J) : 100/0 blends.

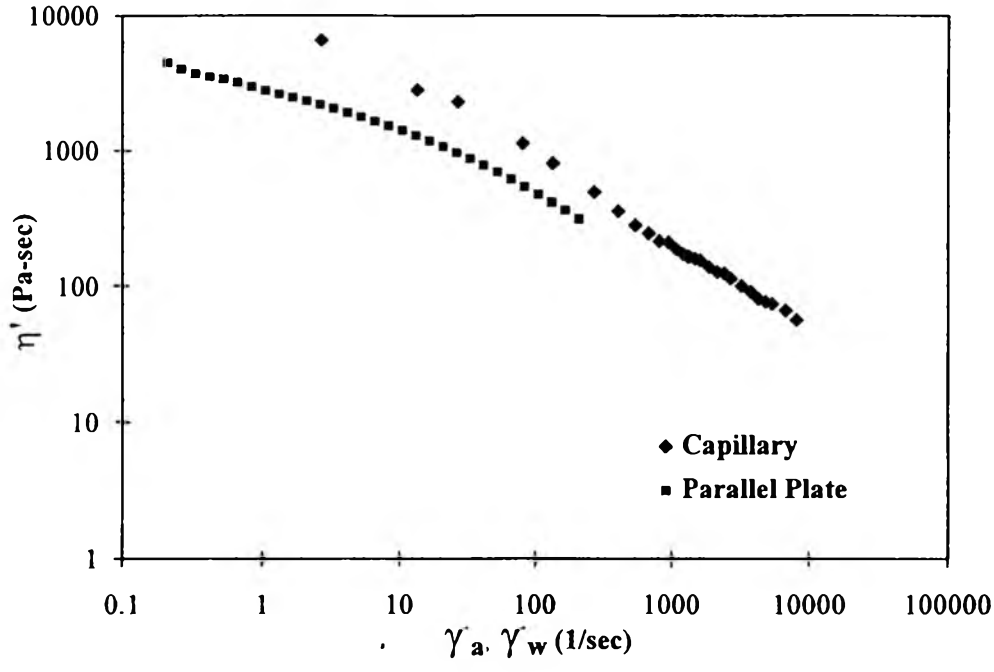

(a)

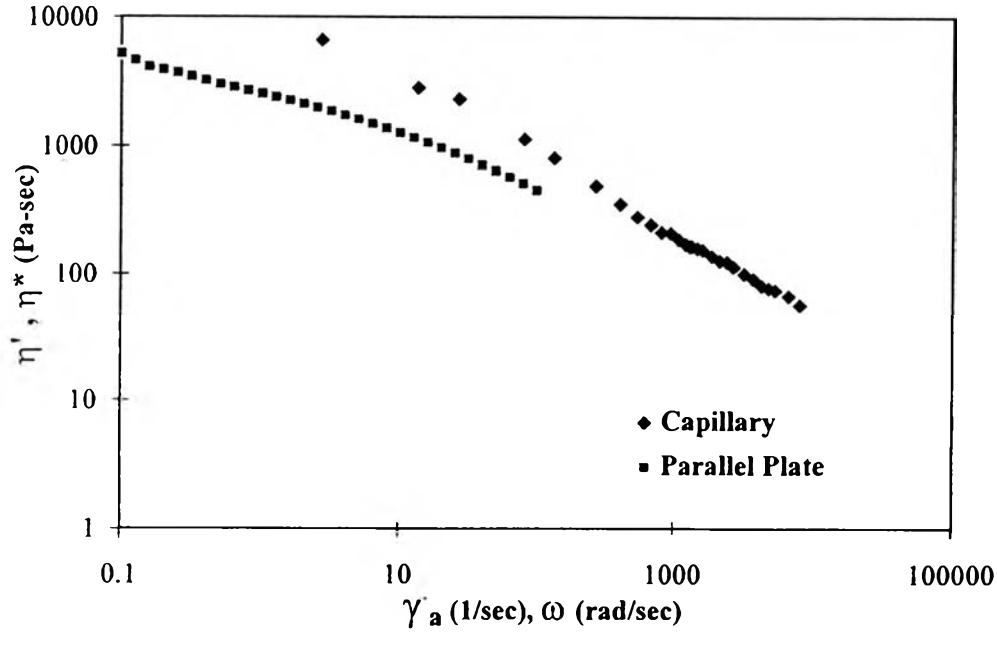

(b)

Figure 3.41 (a) Comparison of the capillary viscosity vs. the apparent strain rate and the parallel plate viscosity vs. the apparent wall strain rate for the HDPE/PP (P340J): 0/100 blends. (b) Comparison of the capillary viscosity vs. the apparent strain rate and the parallel plate complex viscosity vs. the frequency for HDPE/PP (P340J): 0/100 blends.

3.9.2 The Power Law Index

The power law indices of all samples were determined as described in *" Determination of True Viscosity and Power law Index"* of Appendix A at apparent strain rates between 100-2500 1/sec. In this range of strain rate, the melts behaved as non Newtonain fluids obeying the power law relation between viscosity and the strain rate. The results are tabulated in Table 3.10.1. For a blend with n = 1, its melt behaves like a Newtonian fluid. For a blend with n< 1, its melt behaves like a non Newtonian fluid. We can see that HDPE has a lower n value than that of PP; so HDPE melt is more shear thinning. The blend values are found to be bound by the minimum and the maximum values belonging to the pure components. n and K seem to be linear functions of PP content.

Table 3.9.1 Power law index (n) and the constant value (K) of HDPE/PP (P340J) blends

HDPE/PP (P340J) ratio	n	K
0/100	0.358	15399.411
20/80	0.370	16826.725
30/70	0.365	17619.744
40/60	0.359	18685.473
50/50	0.284	33229.152
60/40	0.260	41545.047
70/30	0.208	67068.602
80/20	0.198	96165.248
100/0	0.079	159355.215